

DEFENCE



DÉFENSE

Digital Automatic Gain Control (DAGC) for Surveillance Radar Applications: Theory and Simulation

Michael K. McDonald
Defence Research Establishment Ottawa

DISTRIBUTION STATEMENT A
Approved for Public Release
Distribution Unlimited

20010116 049

Defence R&D Canada

DEFENCE RESEARCH ESTABLISHMENT OTTAWA

TECHNICAL REPORT
DREO TR 2000-115
October 2000



National
Défense
Défense
nationale

Canada

DTIC QUALITY INSPECTED 3



Digital Automatic Gain Control (DAGC) for Surveillance Radar Applications: Theory and Simulation

Michael K. McDonald
*Surveillance Radar Group
Aerospace Radar and Navigation Section*

DEFENCE RESEARCH ESTABLISHMENT OTTAWA

TECHNICAL REPORT
DREO TR 2000-115
October 2000

Project
3DB29

Abstract

The potential for using a digital automatic gain control (DAGC) is examined. The DAGC operates by digitally storing a clutter map of the average of past returns. This average clutter map is digitally filtered to remove small spatial variations and the resulting values are used to adjust the front end receiver gain. In contrast, a traditional analog automatic gain control (AAGC) uses real time filtered feedback to control the adjustable front end gain. The physical realizability constraints of an AAGC typically result in a wider shadow zone for regions where the scan is moving from a land to sea clutter environment. It is shown that the DAGC filtering operation on the clutter map of past returns allows the spatial extent of the filter to be distributed evenly across the land-sea transition regions thereby reducing the shadow zone. The AAGC is shown to display slightly superior noise performance over the DAGC approach. Simulations of the behaviour of both systems under simplified configurations are also shown to qualitatively illustrate and clarify the tradeoffs associated with either approach.

Résumé analytique

On étudie la possibilité d'utiliser une commande numérique de gain automatique (CNGA). La CNGA fonctionne en stockant une carte de la moyenne des précédents retours de fouillis. Cette carte de fouillis est filtrée numériquement afin d'en éliminer les petites variations spatiales. On se sert alors des résultats obtenus pour régler le gain récepteur avant. Par contraste, une commande analogique de gain automatique (CAGA) classique utilise une rétroaction filtrée à temps réel pour régler le gain avant. Les contraintes de réalisabilité physique d'une CAGA produisent généralement une zone d'ombre plus grande pour les régions où le balayage passe d'un environnement de fouillis de sol à un environnement de fouillis d'océan. On remarque que l'opération de filtrage de la CAGA effectuée sur la carte des précédents retours de fouillis permet de distribuer uniformément l'étendue spatiale du filtre d'un côté à l'autre des régions de passage terre-mer, réduisant ainsi la zone d'ombre. Il se révèle que la CAGA présente un niveau de bruit légèrement supérieur à celui de la CNGA. Des simulations du comportement des deux systèmes, accomplies selon des configurations simplifiées, sont également montrées pour illustrer et clarifier qualitativement les avantages et les inconvénients liés à chaque option.

Executive Summary

The development of the digital scan converter (DSC) and its inherent digital processing capabilities opens the door to a variety of different schemes for digitally manipulating scanned data so as to improve the overall detection capability of the AN/APS-506 surveillance RADAR. This report examines one possible technique, namely the implementation of a digital automatic gain control, DAGC, as part of the RADAR system.

The DAGC controls the gain by building a clutter map of the average of the return strengths over time. The clutter map is filtered to remove small spatial variations and the resulting map of large scale variations is used to predict the required attenuation for future incoming returns. Traditionally, RADAR systems have employed an analog automatic gain control system (AAGC), which is essentially a 'hard wired' system. Because of this, it is difficult to adjust an AAGC system during actual operation so as to optimize its performance under different operating modes. This often results in overall performance degradation. The digital approach offers an advantage in this regard since its processing is done digitally and operating parameters can be easily adjusted during operation to allow optimal performance.

This report focuses on the development of the operating theory for both the AAGC and the DAGC. The stability, frequency response and noise characteristics of both systems are examined and compared. In addition, simple simulations are performed to clarify the tradeoffs associated with each system. It is shown that both systems are stable over the full range of realistic operating conditions. The DAGC system is shown to have the most flexible frequency response since the filtering step is performed digitally and the filter shape can be chosen at will. This flexibility allows the DAGC to be interactively adjusted to provide a finer gain control resolution at the land-sea interface thereby reducing the spatial extent of the shadow region that the 'memory' of the strong land clutter returns can cause over the sea. The practical inability of adjusting the RC values of the range gated filters in the AAGC usually results in a relatively large shadow region along the coast. While the AAGC system displays a small superiority in noise performance, the difference is small enough that it is not likely to be a significant factor influencing the choice of system approach.

McDonald, Michael K., Digital Automatic Gain Control (DADC) for Surveillance Radar Applications: Theory and Simulation. Defence Research Establishment Ottawa, DREO TR 2000-115, December 2000.

Sommaire

La mise au point du convertisseur de balayage numérique (CBN) et de ses inhérentes capacités de traitement numérique ouvre la voie à tout un éventail de moyens qui permettent de traiter numériquement des données de balayage pour améliorer la capacité de détection générale du radar de surveillance AN/APS-506. Le présent rapport examine une technique possible, soit la mise en œuvre de la commande numérique de gain automatique, CNGA, intégrée au système radar.

La CNGA règle le gain en élaborant une carte de fouillis représentant la moyenne des forces des retours enregistrées au fil du temps. La carte est filtrée pour éliminer les petites variations spatiales et le résultat, une carte aux grandes variations d'échelle, sert à prévoir l'atténuation requise pour les prochains retours. Jusqu'ici, les systèmes radars ont utilisé un système de commande analogique de gain automatique (CAGA), un système essentiellement « câblé ». De ce fait, il est difficile de régler le système CAGA pendant l'opération proprement dite pour maximiser sa performance dans des modes de fonctionnement différents. Cela entraîne souvent une dégradation de performance générale. Le procédé numérique offre un avantage à cet égard, étant donné que son traitement se fait numériquement et qu'on peut régler facilement les paramètres d'exploitation pendant qu'il fonctionne pour obtenir une performance optimale.

Le présent rapport se focalise sur le développement de la théorie d'exploitation visant les deux systèmes CAGA et CNGA. La stabilité, la réponse en fréquence et les caractéristiques de bruit des deux systèmes sont examinées et comparées. De plus, de simples simulations sont effectuées pour préciser les avantages et les inconvénients associés à chaque système. On note que les deux systèmes s'avèrent stables dans toutes les conditions pratiques d'exploitation. Il se révèle que la réponse en fréquence du système CNGA est la plus souple puisque l'étape de filtrage se fait numériquement et qu'on peut choisir la forme du filtre à volonté. Cette souplesse permet de régler la CNGA de manière interactive pour obtenir une plus haute résolution de la commande de gain à l'interface terre-mer, ce qui réduit l'étendue spatiale de la région d'ombre que la « mémoire » des puissants retours de fouillis de terre peut provoquer sur la zone maritime. Puisqu'il est impossible de pratiquement régler les valeurs de la résistance de capacité des filtres à déclenchement de la CAGA, on obtient généralement une grande région d'ombre le long de la côte. Si le système CAGA présente une efficacité légèrement supérieure quant au bruit, la différence n'est pas assez importante pour être un facteur déterminant notable dans le choix de système.

McDonald, Michael K., Digital Automatic Gain Control (DADC) for Surveillance Radar Applications: Theory and Simulation. , Centre de recherches pour la défense Ottawa, DREO TR 2000-115, décembre 2000. (en anglais)

Table of Contents

Abstract.....	i
Résumé analytique.....	i
Executive Summary.....	iii
Sommaire.....	iv
Table of Contents.....	v
List of Figures.....	vi
List of Tables.....	vii
1.0 Introduction	1
1.1 Receiver Specifications.....	3
2.0 Automatic Gain Control Theory	4
2.1 Analog Automatic Gain Control (AAGC).....	4
2.2 Digital Automatic Gain Control (DAGC).....	9
2.2.1 Transfer Function and Stability of DAGC without Spatial Filtering	10
2.2.2 Noise Performance of DAGC	13
2.2.3 Frequency Responses of DAGC	16
2.2.4 Transfer Function and Stability of DAGC with Spatial Filtering	17
3.0 Simulations	22
3.1 Configuration 1 Simulations - RADAR Sweeping from Sea to Land to Sea.....	25
3.2 Configuration 2 Simulations - RADAR Sweeping Parallel to Land.....	32
4.0 Summary and Future Work	34
References	35
List of Acronyms	36

List of Figures

Figure 1: Typical analog AGC loop implementation.....	1
Figure 2: Proposed configuration of AGC loop.....	2
Figure 3: AGC configuration assumed in report.....	5
Figure 4: Gain control characteristic.	7
Figure 5: Steady state static regulation curves for $u_1=10,150$ and 500	7
Figure 6: Sampling action of range gated filter banks. Dotted line shows impulse response of RC filter in time and dashed lines show how impulse response is distributed in time by range gating action. Solid line is a sample sinusoid input signal. Current output of RGF (TIME = 0) would equal integrated sum of dashed filter response multiplied by sample signal from TIME=0 through to (- Infinity).	8
Figure 7: Bode plot of range gated filter bank and AAGC loop with feedback arm gain, μ_1 , equal to 150. Curves are displayed for average AAGC input signal power levels after input amplification and are as follows: receiver noise = .025 W, sea clutter = 0.65 W and land clutter =6.5 W.	9
Figure 8: Flow chart of simplified DAGC loop without spatial filtering. N equals the number of temporal samples averaged together and REF is the desired reference level.....	10
Figure 9: Noise enhancement factor versus accuracy with which correction can be applied. A=1 represents perfect application of desired gain correction while A<1 represents an underestimate and A>1 an overestimate of the required correction. Curves are shown for cases in which 1, 3 or 10 past scans are averaged to form the gain correction estimate.	14
Figure 10: Step response of simple DAGC loop without spatial filtering for N=1, 3 and 10 scan averaging.	15
Figure 11: Bode plot of DAGC response for N=1, 3 and 10 scan averaging. x-axis is actually $w*T$, to get frequency divide the x-axis values by the sampling period, T.....	16
Figure 12: Flow chart of simplified DAGC loop with spatial filtering. See text for description of variables and subscripts. See figure 8 for loop definitions.....	18
Figure 13: Test configuration 1 to simulate the effect of a radar beam sweeping from sea clutter onto land and back onto sea clutter. Azimuthal bin width is 79m and range bin width is 75m.....	23
Figure 14: Test configuration 2 to simulate the effect of radar beam sweeping parallel to shore with AAGC sampling window of 3.8 μ s straddling land-sea. Azimuthal bin width is 79m and range bin width is 75m.	24
Figure 15: Flow chart for algorithm corresponding to AAGC processing module.....	26
Figure 16: Flow chart for algorithm corresponding to DAGC processing module.....	27
Figure 17: Output from AAGC for configuration 1 deterministic input signal. Arrows identify targets.....	28
Figure 18: Output from AAGC for configuration 1 with non-deterministic input signal added. Arrows identify targets.	28
Figure 19: Plot along azimuthal vector containing targets of DAGC output for configuration 1 with deterministic input data. Arrows indicate targets.....	29
Figure 20: Output from AAGC for configuration 1 deterministic input signal with capacitance reduced by two orders of magnitude in RC filter. Arrows indicate targets.	30
Figure 21: Plot along azimuthal vector containing targets of DAGC output for configuration 1 input data with non-deterministic portion of clutter signal added. Arrows indicate targets.	31
Figure 22: Plot along range vector containing targets of AAGC output for configuration 2 input data with non-deterministic portion of clutter signal added. Arrows indicate targets.	33
Figure 23: Plot along range vector containing targets of DAGC output for configuration 2 input data with non-deterministic portion of clutter signal added. Arrows indicate targets.	33

List of Tables

Table 1.1: Receiver Specifications.....3

Table 2.1: Regulation Characteristics.....6

1.0 Introduction

The inherent range dependence of RADAR returns, coupled with the diverse clutter environments encountered, means that RADAR signal return strengths will commonly span several orders of magnitude. Since the dynamic range of the receivers is typically much smaller it is necessary to provide some form of gain control to compress the received signal into a compatible dynamic range. Traditionally, airborne surveillance RADARs have employed an analog feedback loop configuration to achieve the required automatic gain control (AGC) action. A typical implementation of the analog AGC using the well known closed loop negative feedback configuration is shown in fig 1, where $\beta(\omega)$ represents the filter characteristic of the feedback arm. The voltage controlled variable gain device in fig. 1 can be either an amplifier or attenuator or combination of both as determined by the requirements of the system under consideration.

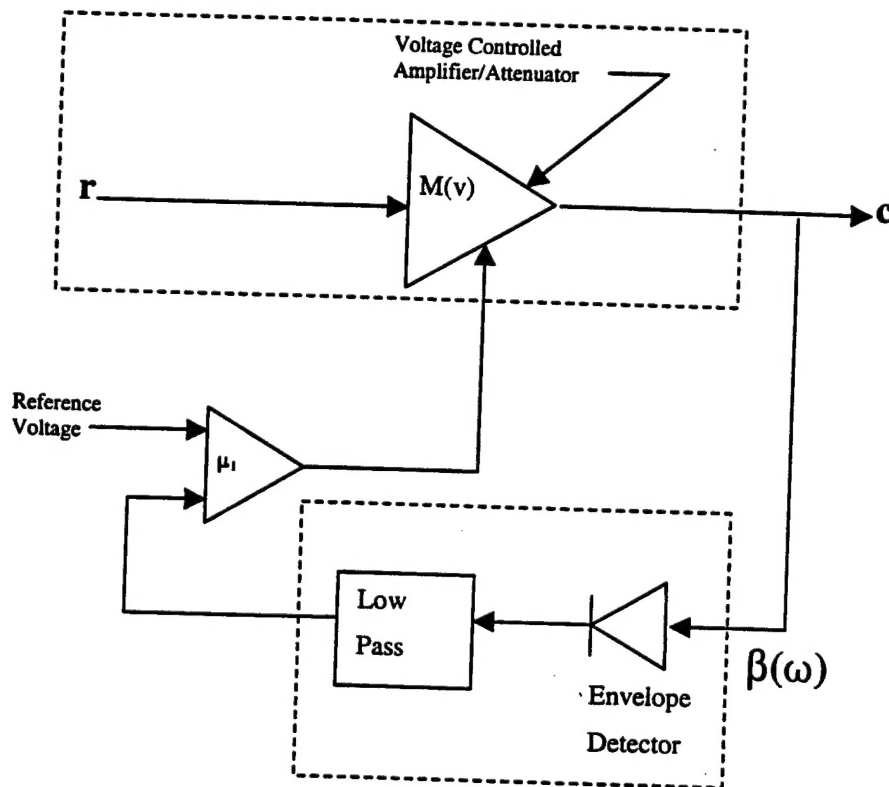


Figure 1: Typical analog AGC loop implementation.

In this report we consider the use of a more elaborate and versatile scheme of AGC made possible by utilizing the digital processing capabilities of the newly developed digital scan converter. To distinguish between the two approaches, the traditional analog automatic gain control will be subsequently referred to as Analog Automatic Gain Control (AAGC) and the digital approach as Digital Automatic Gain Control

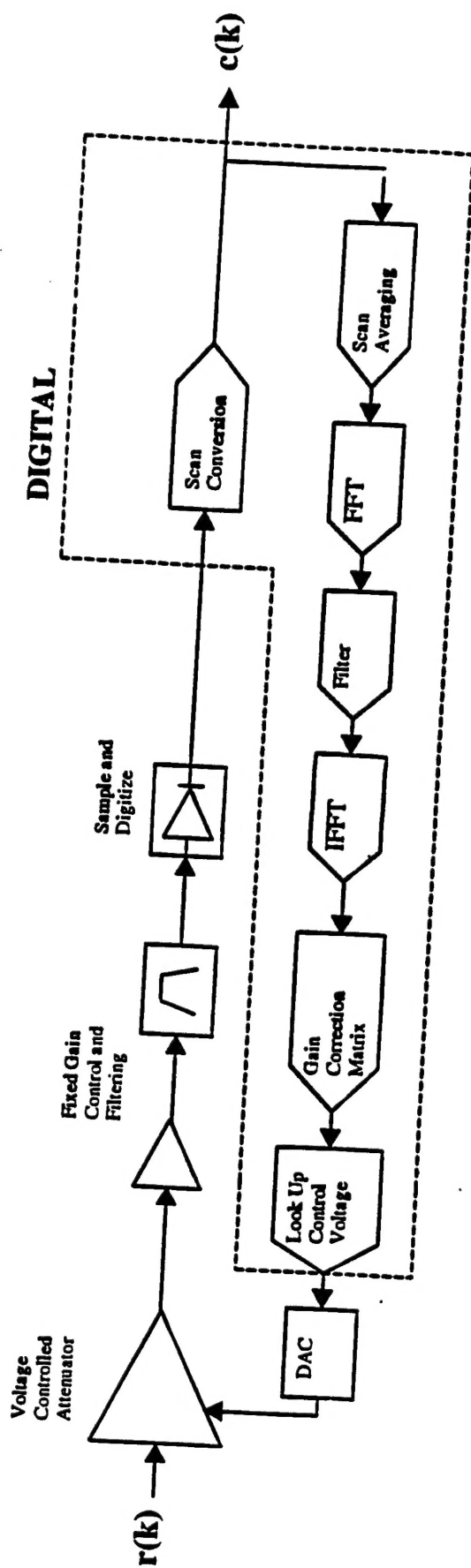


Figure 2: Proposed configuration of digital AGC loop.

(DAGC). The DAGC approach forms an estimate of the required gain for each point by building an average clutter map of the region under consideration over the course of multiple scans. This clutter map can be digitally manipulated to calculate the required gain for returns from each geographic location. The appropriate control voltage is then applied to the controlling amplifier/attenuator to achieve the required gain. The proposed configuration of the DAGC is illustrated in figure 2.

The report is divided into 4 sections. Section 2 summarizes the theory describing the operation of a traditional AGC system and develops the control theory for the proposed DAGC system. In section 3 simulations are run to clarify the performance of the AAGC and DAGC systems. Section 4 summarizes the report and makes recommendations for further work.

1.1 Receiver Specifications

For the purposes of this report simplified AGC configurations are assumed in which only one controlling element is used (i.e. a voltage controlled attenuator). In actual systems, it often proves necessary to place gain control elements throughout the input chain and frequently successive control loops are employed. Nevertheless, the following theory and results are still applicable and it is relatively straightforward to adapt the analysis to these more complex configurations.

Table 1.1 summarizes the nominal receiver specification assumed in this report. Where possible specifications have been derived from the AN/APS-506 surveillance RADAR to ensure a realistic model has been used. Fixed amplification and attenuation stages are assumed inserted throughout the system to meet minimum and maximum signal levels as applicable. The controlling element is assumed to be three cascaded Watkins Johnson G2 voltage controlled attenuators. The choice of an attenuator or amplifier will obviously be system dependent but the theory and results presented in this report are applicable to either configuration.

Table 1.1: RADAR Simulation Parameters

Beamwidth	2.2°	Pulse Repetition Frequency (PRF)	1987 (pulses/sec)
Scanning Rate	300 rpm	Range Resolution	< 1m
Noise Temperature	450K	A to D quantization level	0.0039V
A to D bits & range	8 bits / 1 volt	Antenna Aperture	1.0m * 0.5m
Squint angle	15°	Range	5000 m
Swath width	4800 m	Peak Transmitted Power	500 kW
Noise Bandwidth	500 MHz	Front end gain (pre-AGC)	100 dB

2.0 Automatic Gain Control Theory

2.1 Analog Automatic Gain Control (AAGC)

The theory describing the performance and operation of the traditional AGC loop has been well developed [1] and only a brief summary is given below. Figure 3 illustrates the AAGC configuration assumed in this report. The defining equations for the AAGC loop are easily determined by inspection of figure 3 and are given by

$$c = M(V) * r \quad 2.1$$

and

$$V = c * \mu_1 * \beta(\omega), \quad 2.2$$

where r and c represent the amplitude of the input and output signals respectively, μ_1 is the gain in the feedback arm with the envelope detector assumed to be operating in a linear detection mode, and $\beta(\omega)$ represents the filter characteristic of the feedback arm normalized to one at DC. $M(V)$ represents the voltage amplification factor and is controlled via the feedback arm voltage. Differentiating 2.1 with respect to r , re-arranging and substituting in 2.1 and the derivative of equation 2.2 with respect to M , we obtain

$$\frac{dc}{c} = \frac{1}{1 - \mu_1 \beta(\omega) \frac{c}{M} \frac{dM}{dV}} \frac{dr}{r}. \quad 2.3$$

Linearizing about the DC operating voltage, V_{DC} , we obtain the frequency dependent modulation transfer characteristic

$$\frac{dc}{c} = \frac{1}{1 - \beta(\omega) \frac{V_{DC}}{M} \frac{dM_{DC}}{dV}} \frac{dr}{r}, \quad 2.4$$

where $\frac{dM_{DC}}{dV}$ is the derivative evaluated at V_{DC} .

The subtractor circuit on the attenuator control line in figure 3 converts the attenuator's control characteristic to a positive function i.e. attenuation increases with increasing voltage. The combined control characteristic produced by the G2 attenuator chain and subtractor is plotted in figure 4.

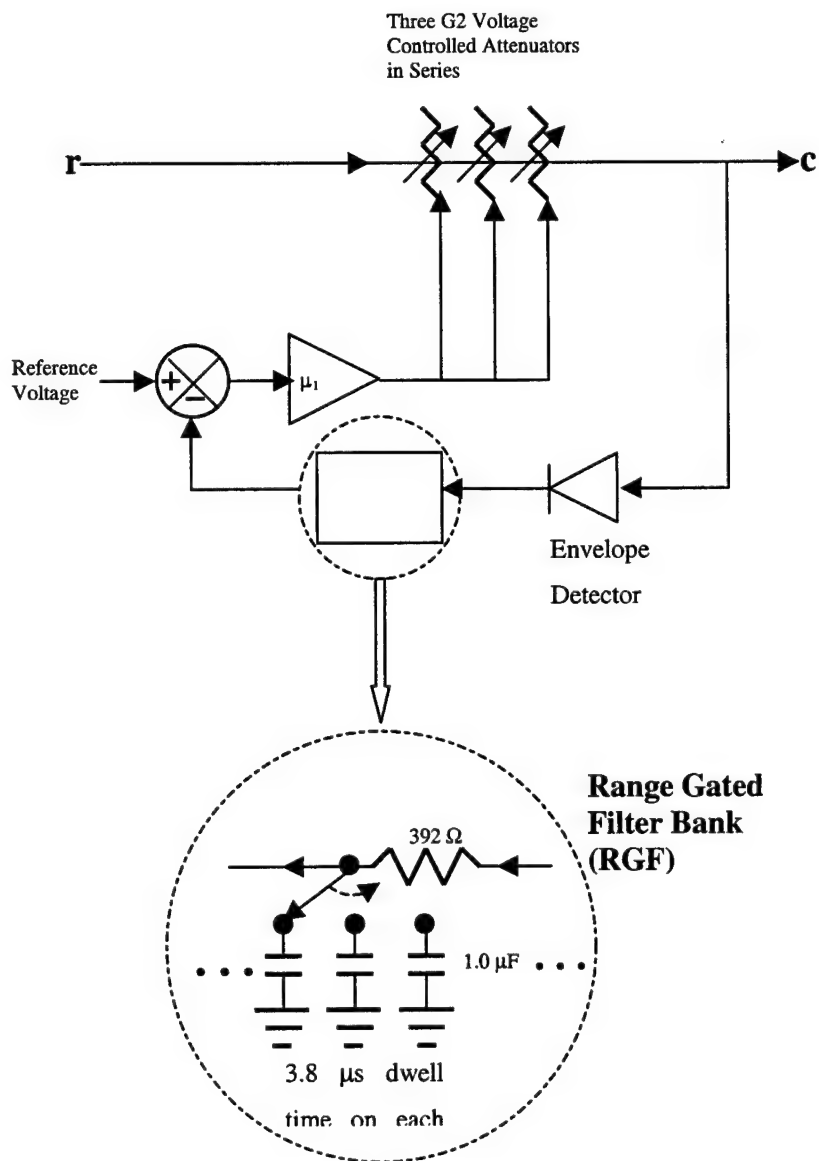


Figure 3: AGC configuration assumed in report.

Table 2.1: Regulation Characteristics

	Input Power (W)	Output Power (W)	Dynamic range between noise and land clutter on output
$\mu_1=10$			
Noise	$2.5 \cdot 10^{-2}$	$7.8 \cdot 10^{-5}$	25 dB
Sea Clutter	$6.5 \cdot 10^{-1}$	$1.8 \cdot 10^{-3}$	
Land Clutter	$6.5 \cdot 10^1$	$2.4 \cdot 10^{-2}$	
$\mu_1=150$			
Noise	$2.5 \cdot 10^{-2}$	$7.8 \cdot 10^{-5}$	5 dB
Sea Clutter	$6.5 \cdot 10^{-1}$	$1.9 \cdot 10^{-4}$	
Land Clutter	$6.5 \cdot 10^1$	$2.5 \cdot 10^{-4}$	
$\mu_1=500$			
Noise	$2.5 \cdot 10^{-2}$	$7.8 \cdot 10^{-5}$	2 dB
Sea Clutter	$6.5 \cdot 10^{-1}$	$9.9 \cdot 10^{-5}$	
Land Clutter	$6.5 \cdot 10^1$	$1.3 \cdot 10^{-4}$	

The static regulation curve of steady state input versus steady state output can now be plotted by calculating the voltage for a given output signal c using the known value of μ_1 , and then reading the corresponding gain from figure 4 to calculate r . $\beta(0)$ is assumed equal to 1. Figure 5 displays the regulation curves for a variety of μ_1 values. Table 2.1 summarizes the input and output power associated with receiver noise, land clutter and sea clutter for the three different feedback arm gains shown in figure 5. All noise is assumed to be Rayleigh distributed with the mean scattering cross-section density assumed to be 0.01 and 0.0001 m^2/m^2 for land and sea clutter, respectively. The input powers are calculated using the parameters listed in table 1.1 and are also used for the simulations carried out in section 3.0. In all cases the impedance has been assumed to be 1 ohm. The choice of front end gain is arbitrary (i.e. gain prior to AGC loop), the important factor is where on the static regulation curve the AAGC is operating. As can be seen in figure 5, a decrease in the front end gain can be compensated for by increasing the feedback arm gain, μ_1 , which results in the static regulation curve being shifted along the slope defined by the unregulated portion of the curve. By judicious choice of μ_1 , the same relative regulation between input and output can be achieved although the absolute value of the input and output will be altered in proportion to the change in the front end gain and thus can be adjusted to meet the power level requirements of the system components. All outputs are normalized so that the average voltage output due to receiver noise alone is equal to two A/D quantization units or 0.0078 V. Using table 2.1 we choose a μ_1 value of 150 as providing a reasonable level of regulation i.e. the 34 dB dynamic range of input between receiver noise and land clutter is compressed to 5 dB on output. This value will be used for subsequent calculations involving the AAGC performance.

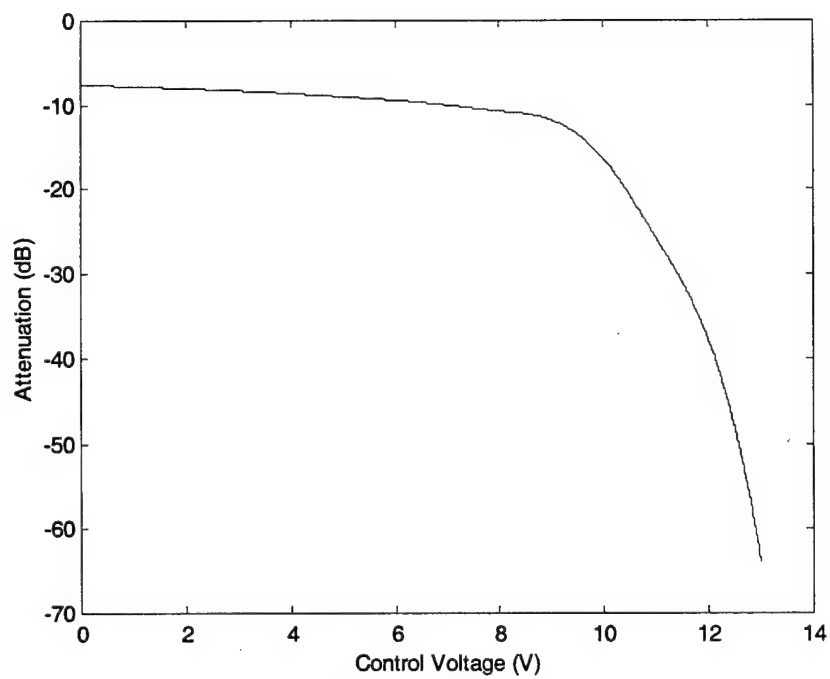


Figure 4: Gain control characteristic.

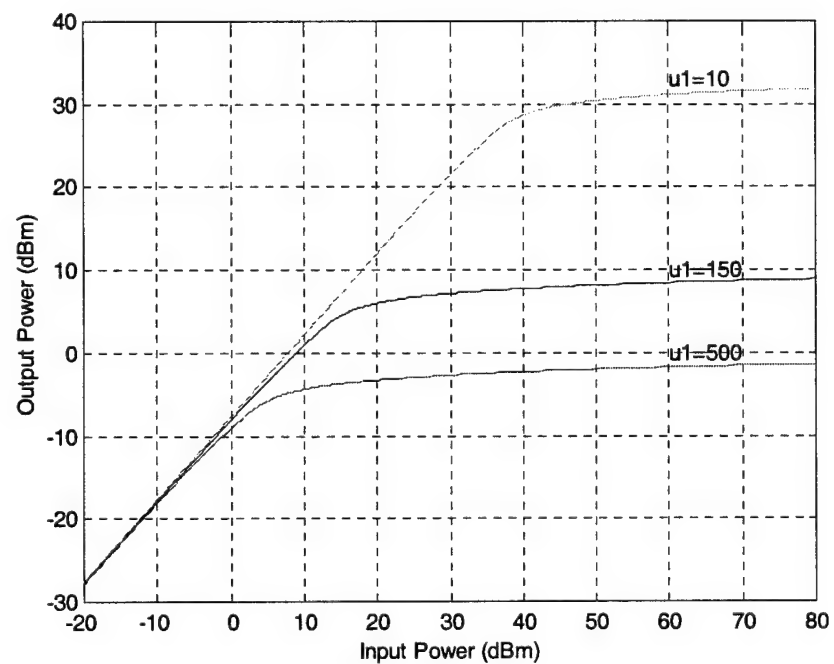


Figure 5: Steady state static regulation curves for $u_1=10, 150$ and 500 .

The frequency behaviour of the AAGC can now be calculated using equation 2.4. In this example, the low pass filtering action in the feedback arm is assumed to be accomplished using a range gated filter (RGF) bank of $1.0 \mu\text{F}$ capacitors attached in parallel to the feedback arm as shown in figure 3. The equivalent circuit is that of a simple RC lowpass filter. This configuration is identical to the RGF currently employed in the AN/APS-506 RADAR. Consistent with the AN/APS-506, each capacitor is assumed gated on for a range interval of $3.8 \mu\text{s}$, and switched to a hold configuration (i.e. input line floating) during the 'off' periods.

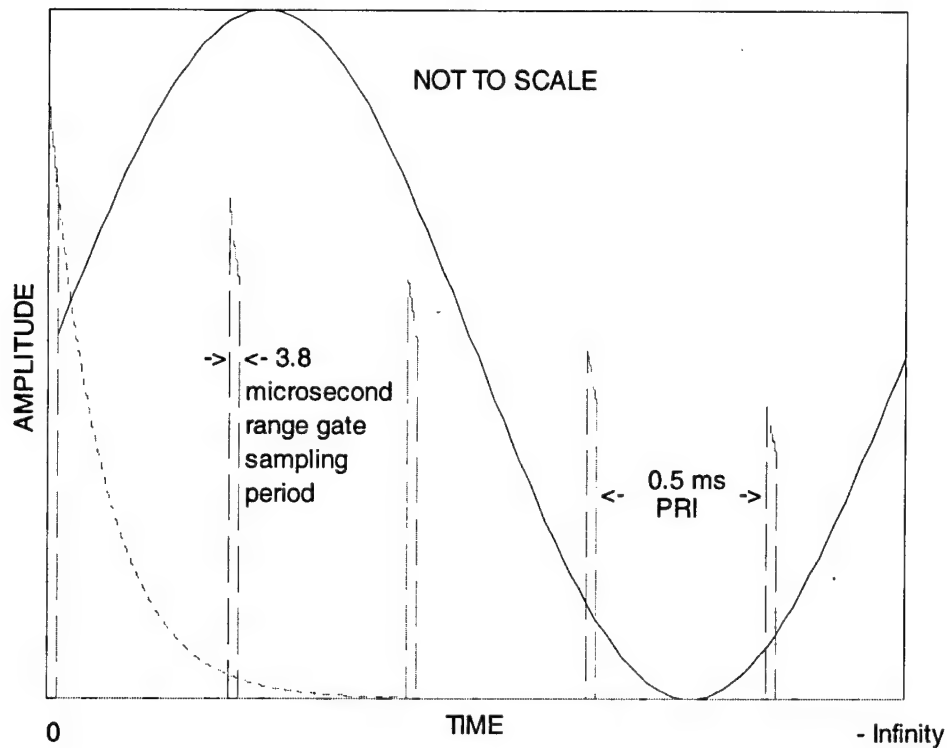


Figure 6: Sampling action of range gated filter banks. Dotted line shows impulse response of RC filter in time and dashed lines show how impulse response is distributed in time by range gating action. Solid line is a sample sinusoid input signal. Current output of RGF (TIME = 0) would equal integrated sum of dashed filter response multiplied by sample signal from TIME=0 through to (-Infinity).

Figure 6 demonstrates the applicable sampling action where the time domain impulse response of the RC filter has been distributed across the discrete time samples by the holding action of the RGF. Figure 7 displays the lowpass behaviour of this range gated filter calculated assuming that each 'on' period can be modeled as an impulse function. This assumption is valid as long as the wavelength is much longer than the length of the range-sampling period. Errors of less than 2.5% are introduced for wavelengths 8 times as long or greater than the sampling window. The corresponding AAGC transfer functions are also shown for

a variety of input signal amplitudes assuming $\mu_1=150$. Because an undelayed AAGC is assumed (i.e. no reference voltage) lower input power signals are more poorly regulated than higher power signals. The overall frequency behavior of the AAGC system is that of a high pass filter, as expected.

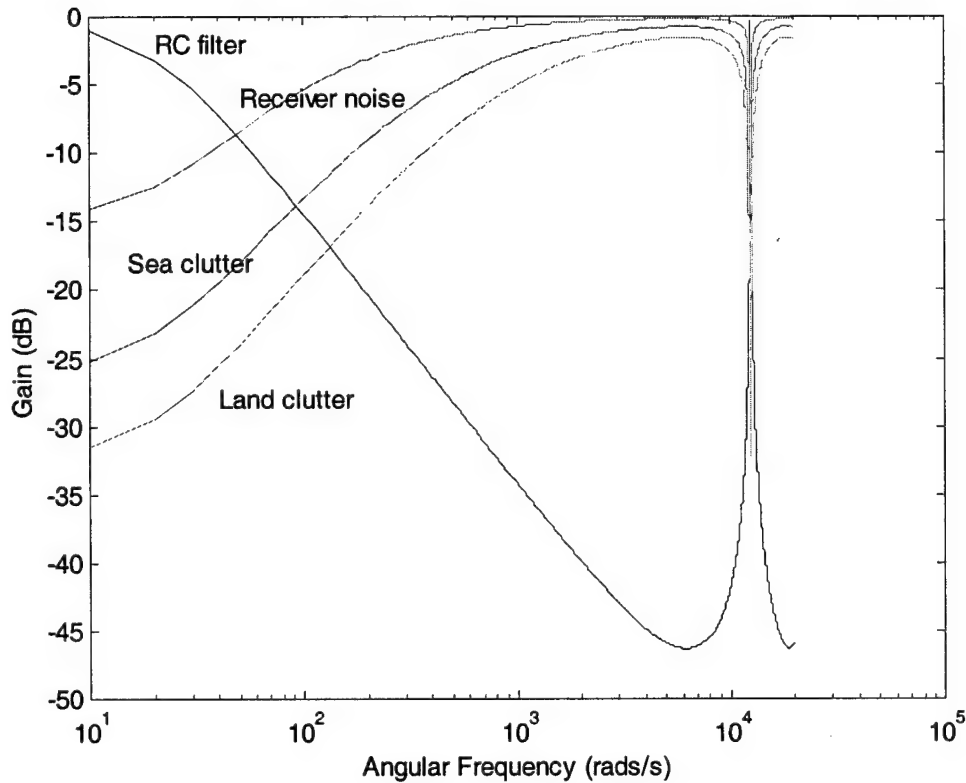


Figure 7: Bode plot of range gated filter bank and AAGC loop with feedback arm gain, μ_1 , equal to 150. Curves are displayed for average AAGC input signal power levels after input amplification and are as follows: receiver noise = .025 W, sea clutter = 0.65 W and land clutter = 65 W.

Clearly the performance of the AAGC is limited by the fixed nature of the RGF, i.e. the capacitors are fixed, and also the relatively slow rolloff of the AAGC frequency response. In particular, the long memory of the AAGC will degrade the performance of the gain control in viewing configurations where the azimuthal movement of the beam is from a strong clutter environment such as land clutter to a weaker sea clutter environment.

2.2 Digital Automatic Gain Control (DAGC)

Figure 2 displays a block diagram describing the proposed operation of the DAGC. RADAR returns entering the DAGC are pulse compressed and mapped to their polar coordinates in memory. This polar coordinate data is then scan converted to a raster format to form a clutter map of the returns. A typical scan

conversion algorithm is described in detail in DREO Report No. 1113 [2] and involves the filtering of the data to prevent aliasing followed by interpolation to the raster grid. The raster data is now available for manipulation by the processors in the DAGC feedback arm. The first stage of manipulation allows the addition of multiple scans to improve the signal to noise ratio of the retrieved clutter map. The averaged raster data is then fast fourier transformed (FFT) from the spatial domain to the frequency domain where it can be digitally filtered as desired by multiplication with a 2-D filter function. The filtered clutter map values are now compared with the desired threshold voltage to determine the gain correction required. In this report the threshold is set equal to two quantization levels of the A to D converter. This represents a compromise between maximizing the dynamic range available for detection while ensuring quantization loss is kept to a reasonable level. As a final step the generated gain control vector is decompressed for application to the adjustable attenuator which is located prior to the pulse compression unit in the input chain.

2.2.1 Transfer Function and Stability of DAGC without Spatial Filtering

Since the DAGC is a digital system sampling the input signal once per time step, the transfer function of the loop is most easily evaluated using the z transform. This can be determined by taking the Laplace transform of the periodic discrete signal and replacing the factor e^{sT} with z , where T is the sampling interval of the signal.

A more detailed description of z -transforms and their applications can be found in [3]. It can be shown that the transfer function of a delay element of one time step is z^{-1} . In order to make the analysis of the system more amenable to standard feedback theory, it is convenient to work with the log of the signals and convert all operations to their log equivalents. Using the above definition, the flow chart of a simplified system without spatial filtering is shown in figure 8. This simplified view is equivalent to modeling the DAGC properties for one geographic location independent of the points surrounding it.

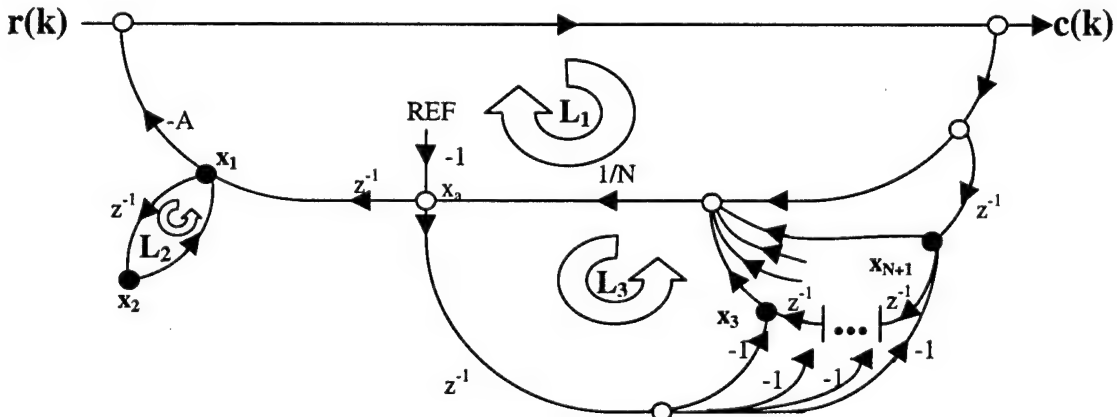


Figure 8: Flow chart of simplified DAGC loop without spatial filtering. N equals the number of temporal samples averaged together and REF is the desired reference level.

Each state variable is identified by a subscript number after the x. Intermediate variables are also shown in the figure, these variables are identified by a letter subscript. These variables are redundant and are not required for the matrix solution, they are introduced simply to facilitate the discussion.

In a real system the averaging process is applied to a non-log signal, i.e.

$$x_a = \frac{(s + d1) + (s + d2) + (s + d3)}{3} = s + \frac{d1 + d2 + d3}{3}. \quad 2.5$$

where we have temporarily set REF = 0 for simplicity. Assuming that the fluctuations, d_i are equal and represent the independent standard deviations of probability distributions governing the noise they are then added in quadrature giving

$$x_a = s + \frac{d}{\sqrt{3}}. \quad 2.6$$

Taking the log we obtain

$$\log(x_a) = \log\left(s + \frac{d}{\sqrt{3}}\right). \quad 2.7$$

In the log converted flow chart we have approximated this averaging process by averaging the log signal directly to give $\text{LOG}x_a$ which can be shown to be roughly equivalent to $\log(x_a)$ provided the fluctuations in d are small compared to the average signal level s . Averaging in the log system gives us

$$\text{LOG}x_a = \frac{[\log(s + d1) + \log(s + d2) + \log(s + d3)]}{3}. \quad 2.8$$

But $\frac{\partial(\log s)}{\partial s} = \frac{1}{s}$, therefore if d_i is small compared to s we can linearize about s to obtain

$$\text{LOG}x_a \approx \frac{\log(s) + \frac{d1}{s} + \log(s) + \frac{d2}{s} + \log(s) + \frac{d3}{s}}{3} = \log(s) + \frac{d1}{3s} + \frac{d2}{3s} + \frac{d3}{3s}. \quad 2.9$$

As above the fluctuations d_i add in quadrature giving

$$LOGx_a \approx \log(s) + \frac{d}{s\sqrt{3}} \approx \log(s + \frac{d}{\sqrt{3}}) = \log(x_a). \quad 2.10$$

The feedback loop in figure 8 can now be analyzed using standard techniques. The families of feedback loops present in the flow chart are identified in figure 8 as L1, L2 and L3 and are listed below.

$$L_1 = \begin{bmatrix} z^{(N-(N-0))} * \frac{1}{N} * (z^{-1}) * (-A) \\ z^{(N-(N-1))} * \frac{1}{N} * (z^{-1}) * (-A) \\ \vdots \\ \frac{-z^{-N} A}{N} \end{bmatrix} = \begin{bmatrix} \frac{-z^{-1} A}{N} \\ \frac{-z^{-2} A}{N} \\ \vdots \\ \frac{-z^{-N} A}{N} \end{bmatrix} \quad 2.11$$

$$L_2 = [z^{-1}] \quad 2.12$$

$$L_3 = \begin{bmatrix} (-z^{-1} z^{-(N-2)} \frac{1}{N}) * (-z^{-1} z^{-(N-3)} \frac{1}{N}) * \dots * (-z^{-1} z^{-(N-N)} \frac{1}{N}) \\ (-z^{-1} z^{-(N-3)} \frac{1}{N}) * \dots * (-z^{-1} z^{-(N-N)} \frac{1}{N}) \\ \vdots \\ -z^{-1} z^{-(N-N)} \frac{1}{N} \end{bmatrix} \quad 2.13$$

where A is a variable introduced to represent the accuracy to which the gain can be adjusted in an actual system, i.e. A=1 would represent the ability to apply perfect corrections. Using Mason's rule [4] the transfer function from r to c is

$$T(r \rightarrow c) = \frac{P(\Delta_k)}{\Delta} \quad 2.14$$

where

$$\Delta = 1 - \sum L_1 + L_2 + \sum L_3, \Delta_k = \Delta + \sum L_1, \text{ and } P = 1 \text{ for forward path.}$$

If the transfer function is to be stable with time then the roots of the denominator must all be less than or equal to zero. Table 2.1 shows the stable range of A values for different values of N. Since the voltage

control curve for the controlling attenuator is well known, the variable A will typically be quite close to 1 and the DAGC will be stable for all values of N.

Table 2.1 Stable range of A for varying N.

N	Range of A for Stable Operation
2	0 - 3
5	0 - 6
10	0 - 11

2.2.2 Noise Performance of DAGC

The output, c_j , from the DAGC after j steps can be written as

$$\begin{aligned}
 c_j &= r_j - Ar_{j-1} + A(A-1)r_{j-2} - A(A-1)^2 r_{j-3} + A(A-1)^3 r_{j-4} \\
 &\quad + \dots (-1)^{j-1} A(A-1)^{j-2} r_1 \\
 &= r_j + \sum_{m=1}^{j-1} (-1)^m A(A-1)^{m-1} r_{j-m}
 \end{aligned} \tag{2.15}$$

where r_j represents the input at each step j.

To calculate the contribution from the independent input noise at each step to the output signal we separate r_j into its signal and noise components, $r_j = s + d_j$. As above, s should be a constant value at any one location and d_j equals the standard deviation of the input noise about this value. Linearizing around s as shown above and adding the noise components quadratically we obtain

$$\begin{aligned}
 d_{out} &= \sqrt{\frac{d_j^2}{s^2} + A^2 \frac{d_{j-1}^2}{s^2} + A^2 (A-1)^2 \frac{d_{j-2}^2}{s^2} + A^2 [(A-1)^2]^2 \frac{d_{j-3}^2}{s^2} + A^2 [(A-1)^3]^2 \frac{d_{j-4}^2}{s^2} + \dots} \\
 &= \sqrt{\frac{d_j^2}{s^2} + \sum_{m=1}^{j-1} A^2 [(A-1)^{m-1}]^2 \frac{d_{j-m}^2}{s^2}}.
 \end{aligned} \tag{2.16}$$

This series quickly converges for values of A within the stability limits of the DAGC system. It should again be emphasized that d_{out} is the log value of the deviation due to noise, i.e. if the log of the constant portion of the output signal is s_{out} then the log output will have a one sigma variation about s_{out} such that

$c = s_{out} \pm d_{out}$. Typically the noise figure is constant so that $d_j = d$. If the attenuator voltage characteristic is also perfectly known then $A=1$ and equation 2.16 reduces to

$$d_{out} = \sqrt{2} \frac{d}{s}. \quad 2.17$$

Figure 9 shows a plot of the output noise enhancement factor (noise in/ noise out) from the DAGC versus A . Figure 9 was produced by iteratively adding numerically generated gaussian noise. Since the log approximation is not used the results in figure 9 will differ slightly from those generated using equation 2.16. Also shown are two curves for the case in which 3 and 10 scans are averaged. The improvement in noise performance that can be achieved by scan averaging is demonstrated for all values of A . The introduction of scan averaging also increases the response time of the feedback loop. Figure 10 demonstrates the response of a DAGC system to a step input with A ranging from 0.75 through to 1.25 for the case of 1, 3 and 10 averaged scans.

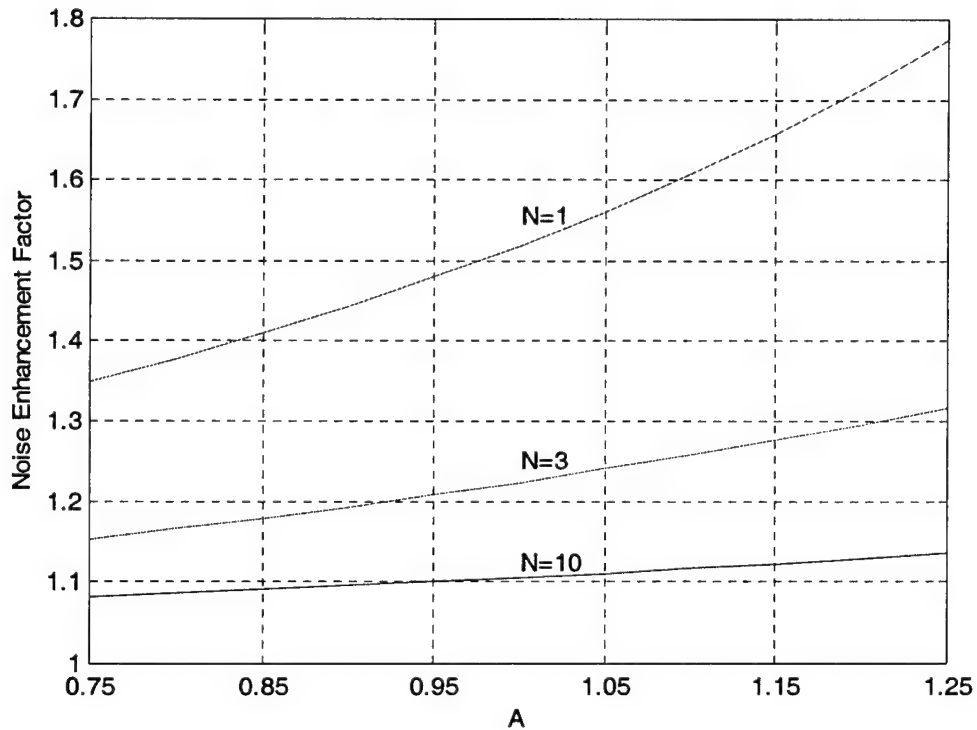


Figure 9: Noise enhancement factor versus accuracy with which correction can be applied. $A=1$ represents perfect application of desired gain correction while $A<1$ represents an underestimate and $A>1$ an overestimate of the required correction. Curves are shown for cases in which 1, 3 or 10 past scans are averaged to form the gain correction estimate.

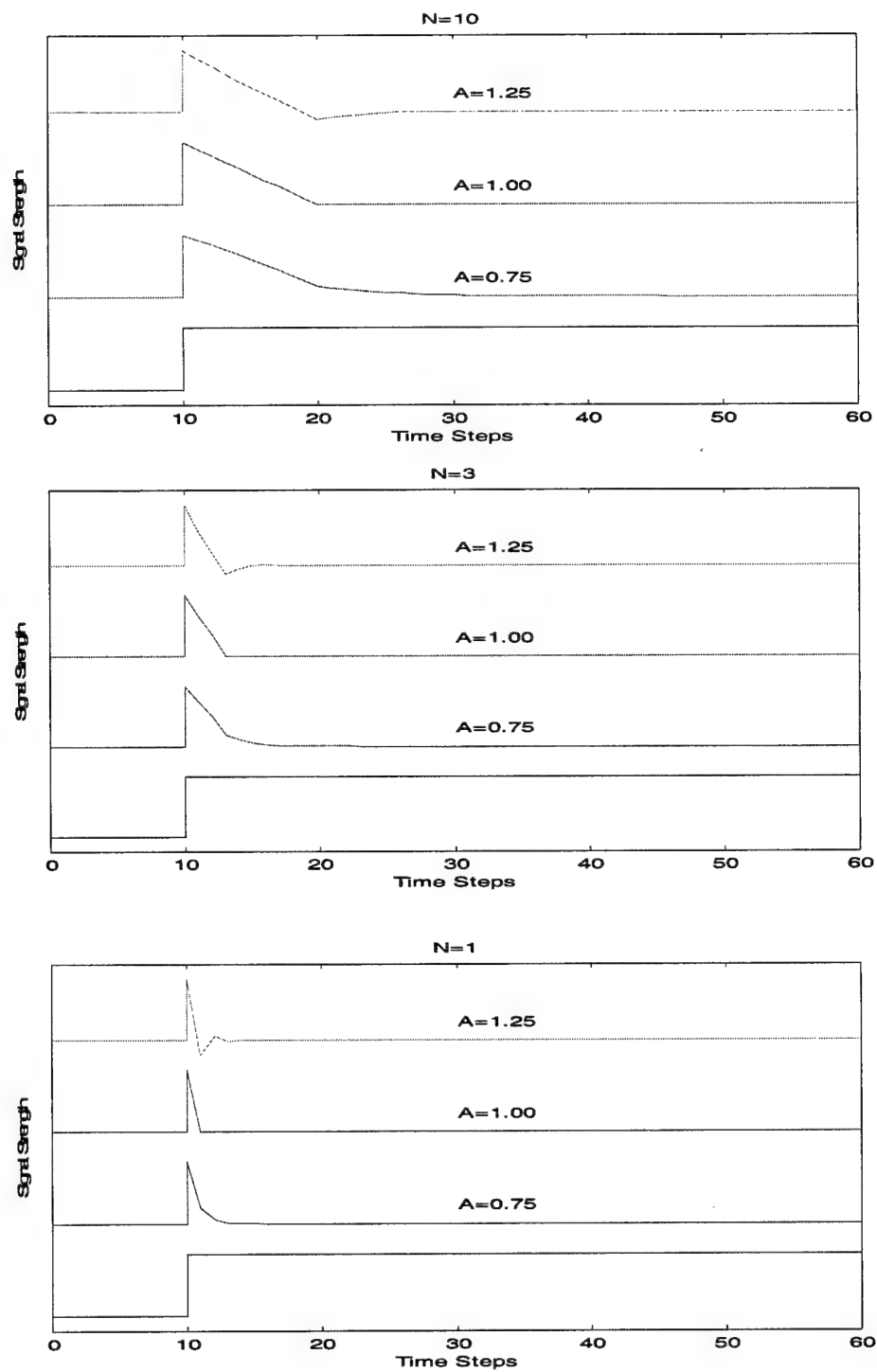


Figure 10: Step response of simple DAGC loop without spatial filtering for $N=1, 3$ and 10 scan averaging.

2.2.3 Frequency Responses of DAGC

The frequency response of the transfer function can be determined using the definition of z and the transformation

$$z = \frac{1 + j\omega_w}{1 - j\omega_w} \quad 2.18$$

where

$$\omega_w = \tan\left(\frac{\omega T}{2}\right)$$

and ω is the angular frequency of the signal.

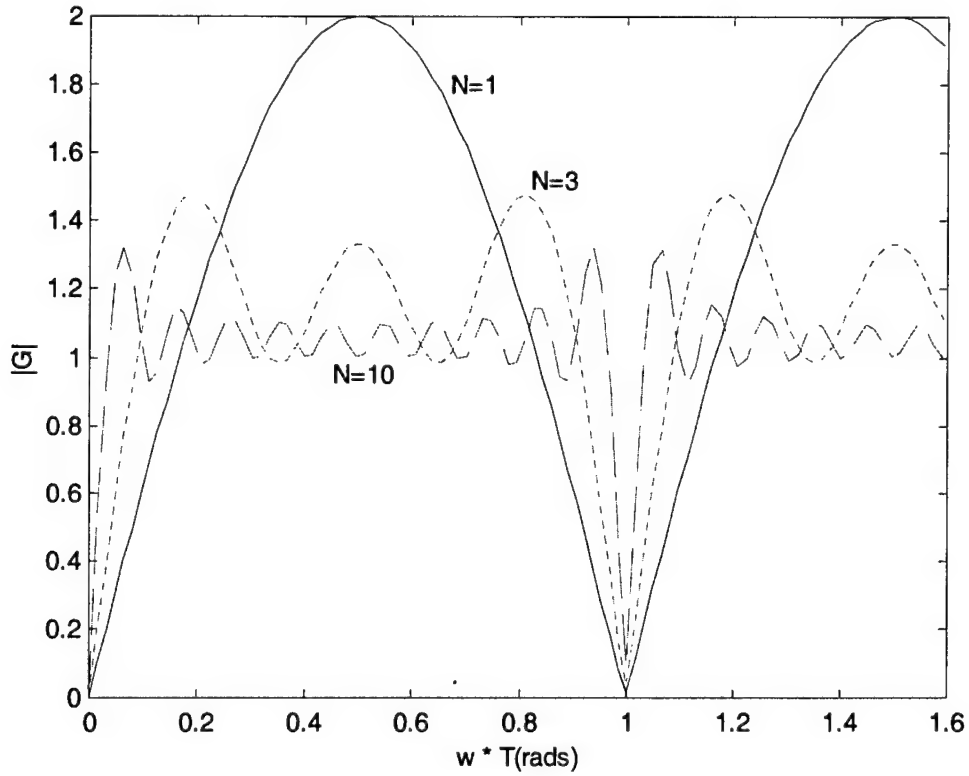


Figure 11: Bode plot of DAGC response for $N=1, 3$ and 10 scan averaging. x-axis is actually $\omega * T$, to get frequency divide the x-axis values by the sampling period, T .

The frequency responses of the loop for different values of N are shown in fig 11. The curves in fig. 11 show that as the number of scans averaged is increased the cutoff of the frequency response is pushed to lower frequencies. It should be emphasized that this frequency response refers to the temporal behaviour of the DAGC for the returns from one geographic location i.e. from scan to scan how does the return at one point on the clutter map vary with time. As might be expected the frequency response displays a periodicity with ω which could result in aliasing for an insufficiently sampled figure.

2.2.4 Transfer Function and Stability of DAGC with Spatial Filtering

The introduction of spatial filtering across the imaged scene rapidly increases the complexity and computational load required to solve for the transfer function. A state variable technique is used below to solve the problem. Figure 12 illustrates the flow chart for one arm of the overall flow chart corresponding to the input to output for one location, i , on the clutter map. Similar flow charts will exist for each location on the clutter map. The arms are coupled together through weighted averaging in the feedback section of each arm. There are $N+1$ state variables associated with each arm. Each variable is identified by a number after the x and a subscript to identify the arm or spatial location to which the state variable belongs. Intermediate variables are also shown in the figure, these variables are identified by a letter subscript. These variables are redundant and are not required for the matrix solution, they are introduced simply to facilitate the discussion. The coupling to other arms occurs at point $x_{b,i}$ where the scan averaged values are fed to the other arms of the overall flow chart. Likewise, variable $x_{c,i}$ corresponds to the value formed from the weighted addition of $x_{b,i}$ with the x_b values from other arms. The choice of weighting function applied determines the spatial filtering applied to the feedback signal. In the actual systems this step would probably be accomplished by the computationally more efficient method of performing a 2D FFT of the map of x_b variables and then applying a 2D filter in the frequency domain.

The general form of the dynamic equations for the system is

$$\mathbf{x}[(j+1)T] = \mathbf{A}\mathbf{x}(jT) + \mathbf{B}\mathbf{u}(jT) \quad 2.19$$

$$\mathbf{c}(jT) = \mathbf{D}\mathbf{x}(jT) + \mathbf{E}\mathbf{u}(jT) \quad 2.20$$

where \mathbf{x} is the matrix of state variables, \mathbf{u} is the matrix of inputs, \mathbf{c} is the matrix of outputs and \mathbf{A} , \mathbf{B} , \mathbf{D} and \mathbf{E} are defined below. In the above j represents the time step index. In the subsequent equations the subscript i will be identified with the branch of the output variable under consideration while k will be associated with the branch of the variable acting as an input to the system. N represents the number of scans averaged on any one branch and m represents the number of branches or inputs into (and in this analysis, outputs from) the system. REF represents the desired reference level.

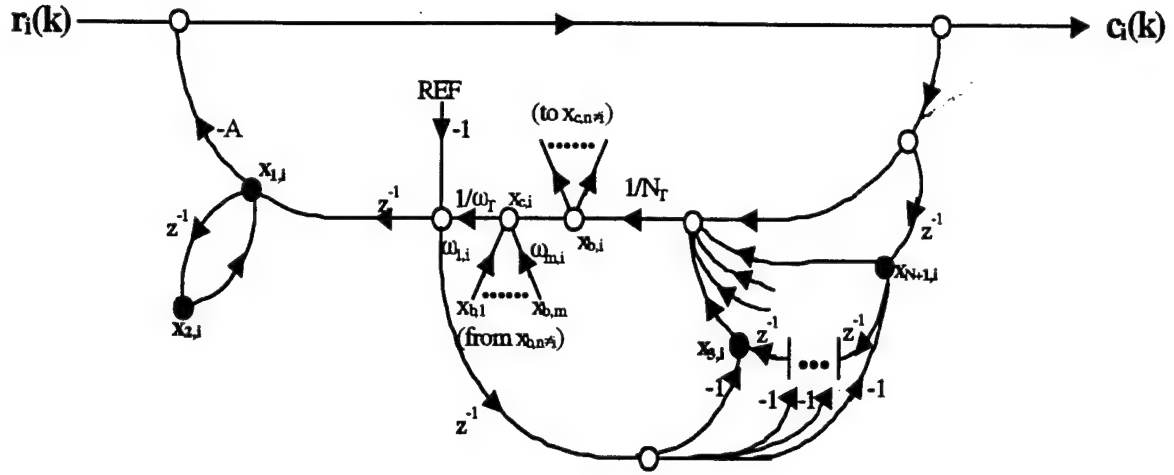


Figure 12: Flow chart of simplified DAGC loop with spatial filtering. See text for description of variables and subscripts. See figure 8 for loop definitions.

Each of the matrices in equations 2.19 and 2.20 can be determined by inspection of the flowchart in fig. 12 and are as follows. \mathbf{x} is given by

$$\mathbf{x} = \begin{bmatrix} x_1 \\ x_2 \\ \vdots \\ x_m \end{bmatrix}$$

where \mathbf{x}_k is

$$\mathbf{x}_k = \begin{bmatrix} x_{1k} \\ x_{2k} \\ \vdots \\ x_{N+1k} \end{bmatrix}$$

x_{1k} through x_{N+1k} represent the state variables for branch k . \mathbf{A} has the dimensions $m^*(N+1)$ by $m^*(N+1)$ and can be formed by examination of figure 12 giving

$$A = \begin{bmatrix} a_{1,1} & a_{1,2} & \dots & a_{1,m} \\ a_{2,1} & a_{2,2} & \dots & a_{2,m} \\ \vdots & \vdots & \ddots & \vdots \\ a_{m,1} & a_{m,2} & \dots & a_{m,m} \end{bmatrix}$$

where $a_{i,k}$ has the dimensions $N+1$ by $N+1$ and is given by

$$a_{i,k} = \begin{bmatrix} -\omega_{i,k} A w_{N+2} & 0 & \omega_{i,k} w_3 & \omega_{i,k} w_4 & \dots & \omega_{i,k} w_N & \omega_{i,k} w_{N+1} \\ 0 & 0 & 0 & 0 & \dots & 0 & 0 \\ \omega_{i,k} A w_{N+2} & 0 & -\omega_{i,k} w_3 & -\omega_{i,k} w_4 & \dots & -\omega_{i,k} w_N & -\omega_{i,k} w_{N+1} \\ \vdots & \vdots & \vdots & \vdots & \ddots & \vdots & \vdots \\ \omega_{i,k} A w_{N+2} & 0 & -\omega_{i,k} w_3 & -\omega_{i,k} w_4 & \dots & -\omega_{i,k} w_N & -\omega_{i,k} w_{N+1} \end{bmatrix} + [a_{off}].$$

The subscript on the w identifies the state variable it is associated with. a_{off} also has the dimensions $N+1$ by $N+1$ and is given by

$$a_{off} = \begin{bmatrix} 1 & 0 & 0 & 0 & 0 & \dots & 0 \\ 1 & 0 & 0 & 0 & 0 & \dots & 0 \\ 0 & 0 & 0 & 1 & 0 & \dots & 0 \\ 0 & 0 & 0 & 0 & 1 & \dots & 0 \\ \vdots & \vdots & \vdots & \vdots & \vdots & \ddots & \vdots \\ 0 & 0 & 0 & 0 & 0 & \dots & 1 \\ -A & 0 & 0 & 0 & 0 & \dots & 0 \end{bmatrix} \quad \text{if } i=k$$

and

$$a_{off} = 0 \quad \text{if } i \neq k.$$

In the above it has been assumed that all branches use the same scan to scan averaging coefficients w_i . In addition both ω and w coefficients are assumed to have been normalized by their respective factors of $1/\omega_T$ and $1/w_T$ as shown in figure 12.

B has the dimensions $m*(N+1)$ by $m+1$ and is given by

$$B = \begin{bmatrix} b_1 \\ b_2 \\ \vdots \\ b_m \end{bmatrix}$$

where

$$b_i = \begin{bmatrix} \omega_{i,1} w_{N+2} & \omega_{i,2} w_{N+2} & .. & \omega_{i,m} w_{N+2} & -1 \\ 0 & 0 & .. & 0 & 0 \\ -\omega_{i,1} w_{N+2} & -\omega_{i,2} w_{N+2} & .. & -\omega_{i,m} w_{N+2} & 1 \\ -\omega_{i,1} w_{N+2} & -\omega_{i,2} w_{N+2} & .. & -\omega_{i,m} w_{N+2} & 1 \\ \vdots & \vdots & :: & \vdots & \vdots \\ -\delta_{i,k} \omega_{i,1} w_{N+2} & -\delta_{i,k} \omega_{i,2} w_{N+2} & .. & -\delta_{i,k} \omega_{i,m} w_{N+2} & 1 \end{bmatrix}$$

where k refers to the column of matrix b_i , $\delta_{i,k}=1$ if $i=k$ and $\delta_{i,k}=0$ if $i \neq k$. \mathbf{u} is an $m+1$ by 1 matrix and is given by

$$\mathbf{u} = \begin{bmatrix} r_1 \\ r_2 \\ \vdots \\ r_m \\ REF \end{bmatrix}.$$

\mathbf{D} is given by

$$D = [D_1 \quad D_2 \quad .. \quad D_m]$$

where D_k has the dimensions m by $N+1$ and is given by

$$D_k = \begin{bmatrix} -A\delta_{i,k} & 0 & 0 & .. & 0 \\ -A\delta_{i,k} & 0 & 0 & .. & 0 \\ \vdots & \vdots & \vdots & :: & \vdots \\ -A\delta_{i,k} & 0 & 0 & .. & 0 \end{bmatrix}$$

where the subscript i refers to the row of the matrix, $\delta_{i,k}=1$ if $i=k$ and $\delta_{i,k}=0$ if $i \neq k$. The matrix E has the dimensions m by $m+1$ and is given by

$$E = \begin{bmatrix} 1 & 0 & \dots & 0 & 0 \\ 0 & 1 & \dots & 0 & 0 \\ \vdots & \vdots & \ddots & \vdots & \vdots \\ 0 & 0 & \dots & 1 & 0 \end{bmatrix}.$$

It can be shown [3] that the transfer function of the system, $G=c/r$ is given by

$$G(z)=[D(zI-A)^{-1}B+E]. \quad 2.21$$

Once the transfer function of the system has been determined the stability of the system can be affirmed in the usual manner by checking if the absolute roots of the denominator in equation 2.21 are less than one i.e. $|z| < 1$.

3.0 Simulations

In order to illustrate the differences between an AAGC and DAGC system, a series of simulations were performed. As stated earlier it is anticipated that the main advantage of the DAGC system will occur along regions such as shorelines where the AAGC can suffer residual affects from the large scattering cross section of the land clutter as the beam sweeps from the land onto the ocean surface. Figures 13 and 14 illustrate the two viewing configurations simulated in this section. The first configuration is chosen to simulate a sector viewing operation where the beam sweeps from sea onto land and back onto sea again. The second configuration simulates the effect of the beam sweeping parallel to the shore with the range bins corresponding to the target range remaining equidistant from the land-sea transition. The average range in both cases is assumed to be 5 km and the change of azimuthal sample spacing with range is insignificant (i.e. has little effect on the results) over the swath width under consideration and is assumed constant for these simulations. To further simplify the simulations other complicating factors such as pulse compression, peak detection, beam width etc. are ignored. Range dependence of the returns across the swath width is also ignored.

All clutter in these simulations is assumed to be Rayleigh distributed with the mean scattering cross section varied as necessary to represent land versus sea clutter. Land clutter is assumed to have a scattering cross section density of $0.01 \text{ m}^2/\text{m}^2$ while sea clutter is assumed equal to $0.0001 \text{ m}^2/\text{m}^2$. The discrete targets in the scene are assumed to have a cross section of 1 m^2 . To reduce the computational load, range samples are generated every 75 m i.e. 64 range intervals over the 4800 m wide swath. However a range interval length of less than one meter is still assumed during the calculation of the clutter viewing area and the corresponding clutter signal strengths to preserve the clutter to signal ratios which would be expected in an actual high resolution RADAR. For each case the equivalent of 200 scans were generated, with the random noise generator re-seeded for each scan. These scans are consecutively processed as per the appropriate algorithm to simulate the AAGC and DAGC systems. The applicable algorithms for the AAGC and DAGC simulators are shown in the block diagrams of figures 15 and 16 respectively. The final output is generated using the simple recursive formula

$$\text{Output Image} = \alpha * \text{new scan} + (1-\alpha) * \text{old scan} \quad 3.1$$

with $\alpha=0.025$.

For all cases an appropriate amplification has been applied to the AAGC output to ensure that the output due to receiver noise alone would equal two quantization units of an 8 bit, 1 volt range AtoD (i.e. $1/255 \text{ V}$). The same desired quantization level is automatically implemented within the threshold comparison step of DAGC processing where the threshold has been specified at the same value.

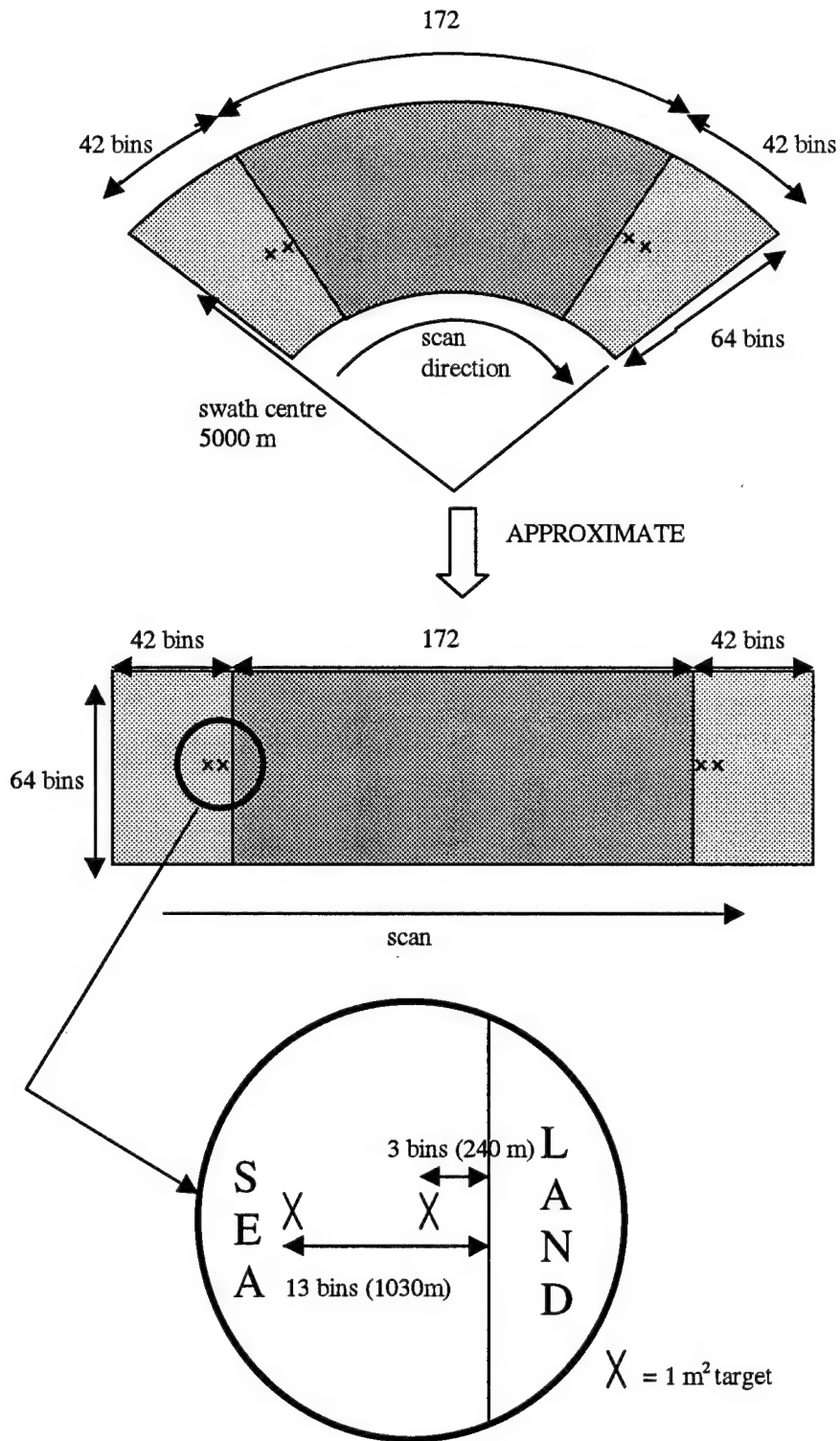


Figure 13: Test configuration 1 to simulate the effect of a radar beam sweeping from sea clutter onto land and back onto sea clutter. Azimuthal bin width is 79m and range bin width is 75m.

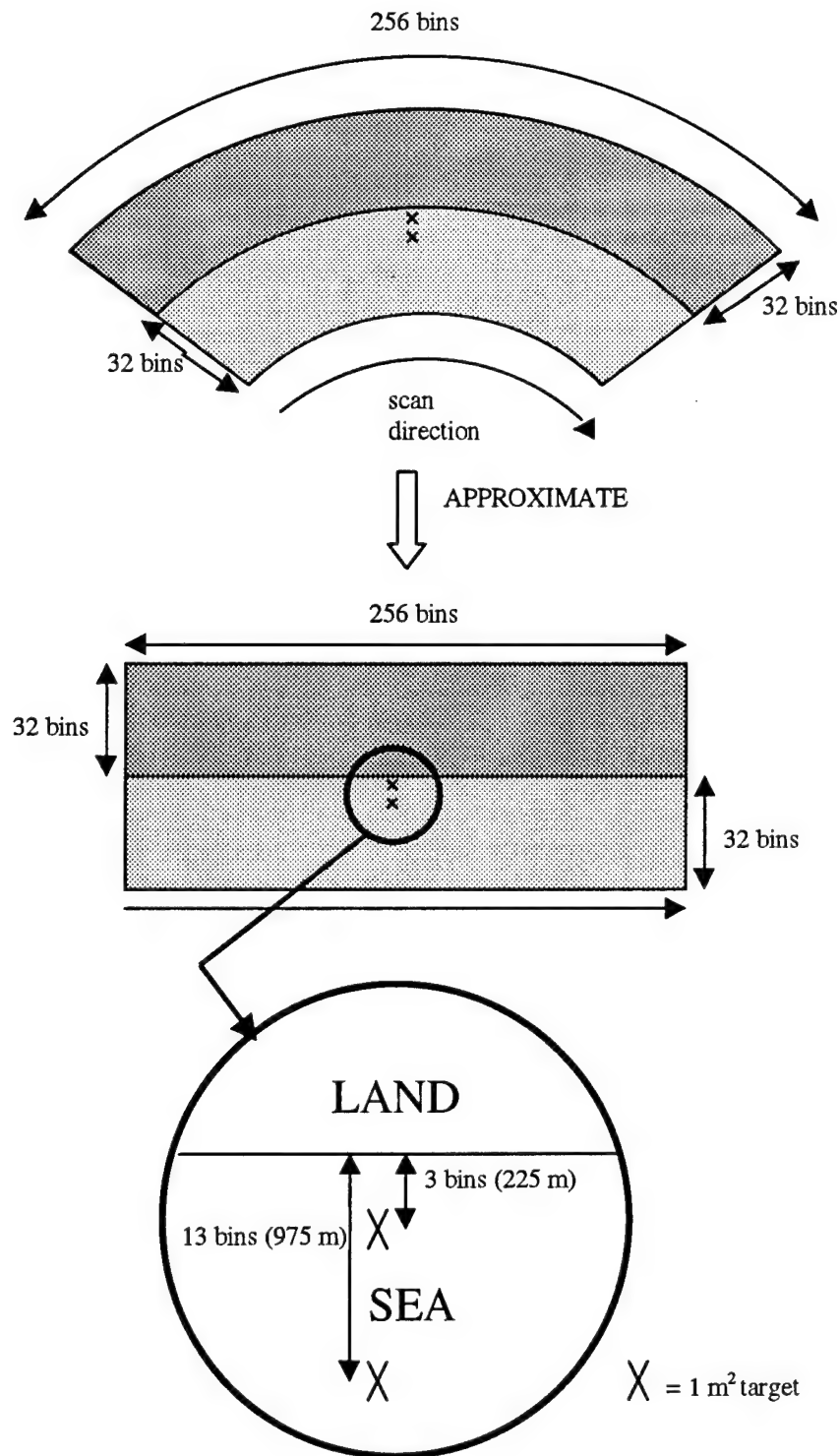


Figure 14: Test configuration 2 to simulate the effect of radar beam sweeping parallel to shore with AAGC sampling window of $3.8 \mu\text{s}$ straddling land-sea. Azimuthal bin width is 79m and range bin width is 75m.

3.1 Configuration 1 Simulations - RADAR Sweeping from Sea to Land to Sea

Figure 17 illustrates the output from the AAGC loop for configuration 1 input data. To clarify the discussion the return signal from the land and sea clutter has been divided into a deterministic portion corresponding to the mean return expected from the land and sea clutter and a non-deterministic portion corresponding to the fluctuations about this mean. Figure 17 shows only the deterministic portions of the clutter signals and the target signals. The AAGC loop configuration assumed was described previously and is illustrated in figure 3, the capacitance and resistance of the RC filter components are $1\ \mu\text{F}$ and $392\ \Omega$ respectively with three cascaded G2 attenuators providing the gain control. Unless otherwise specified the feedback arm gain, μ_1 , is 150.

The movement of the RADAR beam is from left to right in figure 17, the lag in the response of the AAGC on the trailing edge of the land to sea clutter transition is readily apparent with significant masking of the targets located at approximately 17.1 and 17.9 km (azimuthal bin locations 217 and 227). For this example the AAGC output does not recover to the 90% steady state value until the beam has moved a distance of approximately 2.4 km or 30 azimuthal bins from the land to sea transition.

Examination of the leading edge for the sea to land transition reveals a similar lagging response as evidenced by the large spike starting at 3.3 km (azimuthal bin 43). However since this lag occurs over the land where we are not searching for targets it does not degrade the detection performance, in fact due to the non-anticipatory nature of the AAGC and its simple RC filter we achieve single bin azimuthal resolution of targets on the leading edge.

The difficulty of identifying targets in the trailing zone of the land to sea transition is illustrated in figure 18 where the non-deterministic portion of the sea and land clutter responses has been added to the output signal. It is clear in figure 18 that the non-deterministic portion masks the already weak target responses seen in figure 17. The plotted output is derived using an alpha of 0.025 in equation 3.1.

Figure 19 displays the output from the DAGC loop. It should be noted that the DAGC process is actually a two dimensional one as the gain matrix correction applied is generated by performing a two dimensional filtering operation on the clutter map built up over the previous scans. In the following examples we have assumed a simple 2-D circular box filter with a radius of 200 m. For clarity we have extracted one azimuthal vector at the target range from the overall output matrix. The most obvious characteristic of the DAGC response is the symmetrical response of output between the two land-sea interfaces. This is expected due to the spatial filtering operation on the clutter map. The use of a 200m box filter results in a clear identification of targets on the leading and trailing edges of the land-sea transitions, including the targets located 225m from shore. This is in

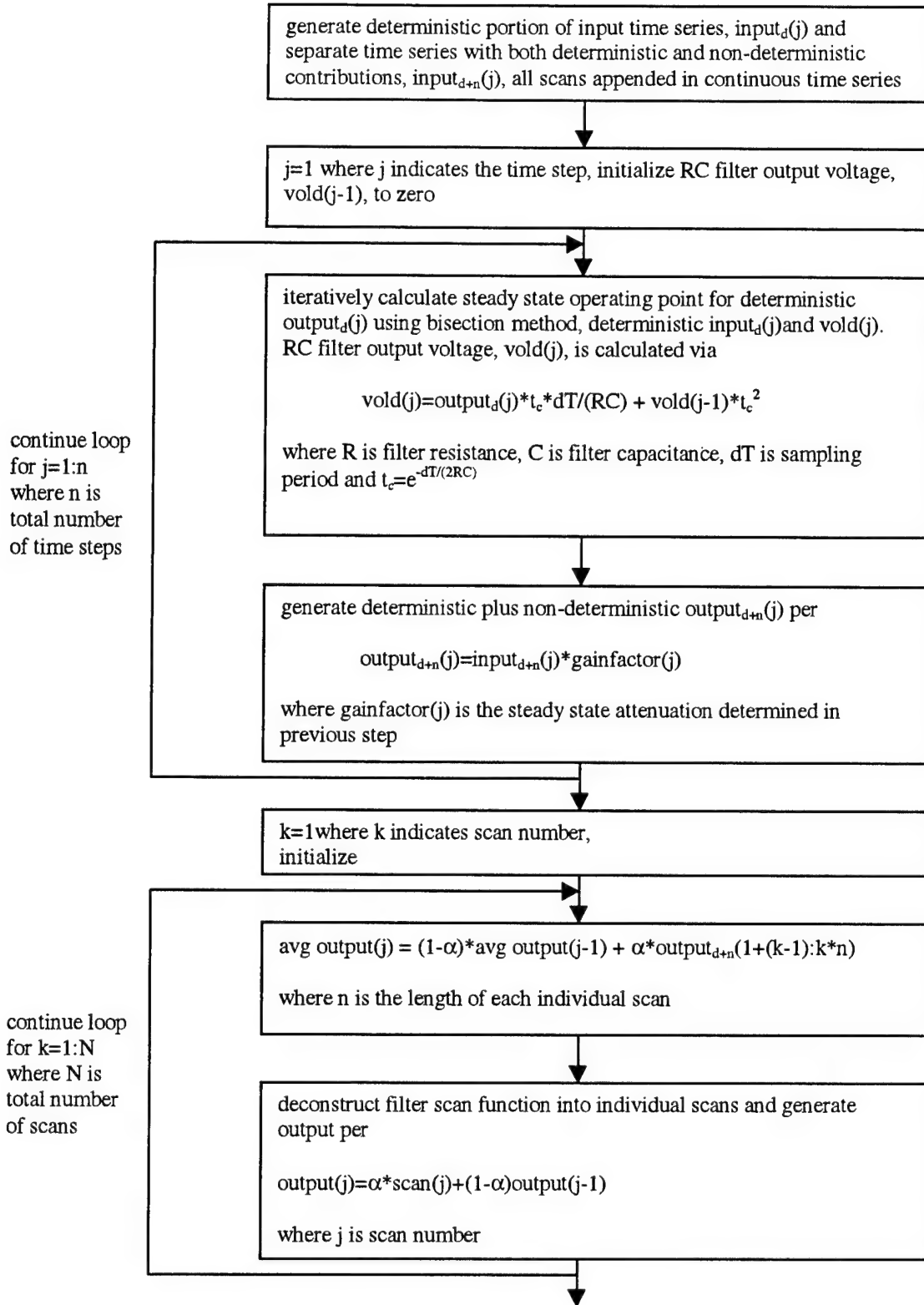


Figure 15: Flow chart for algorithm corresponding to AAGC processing module.

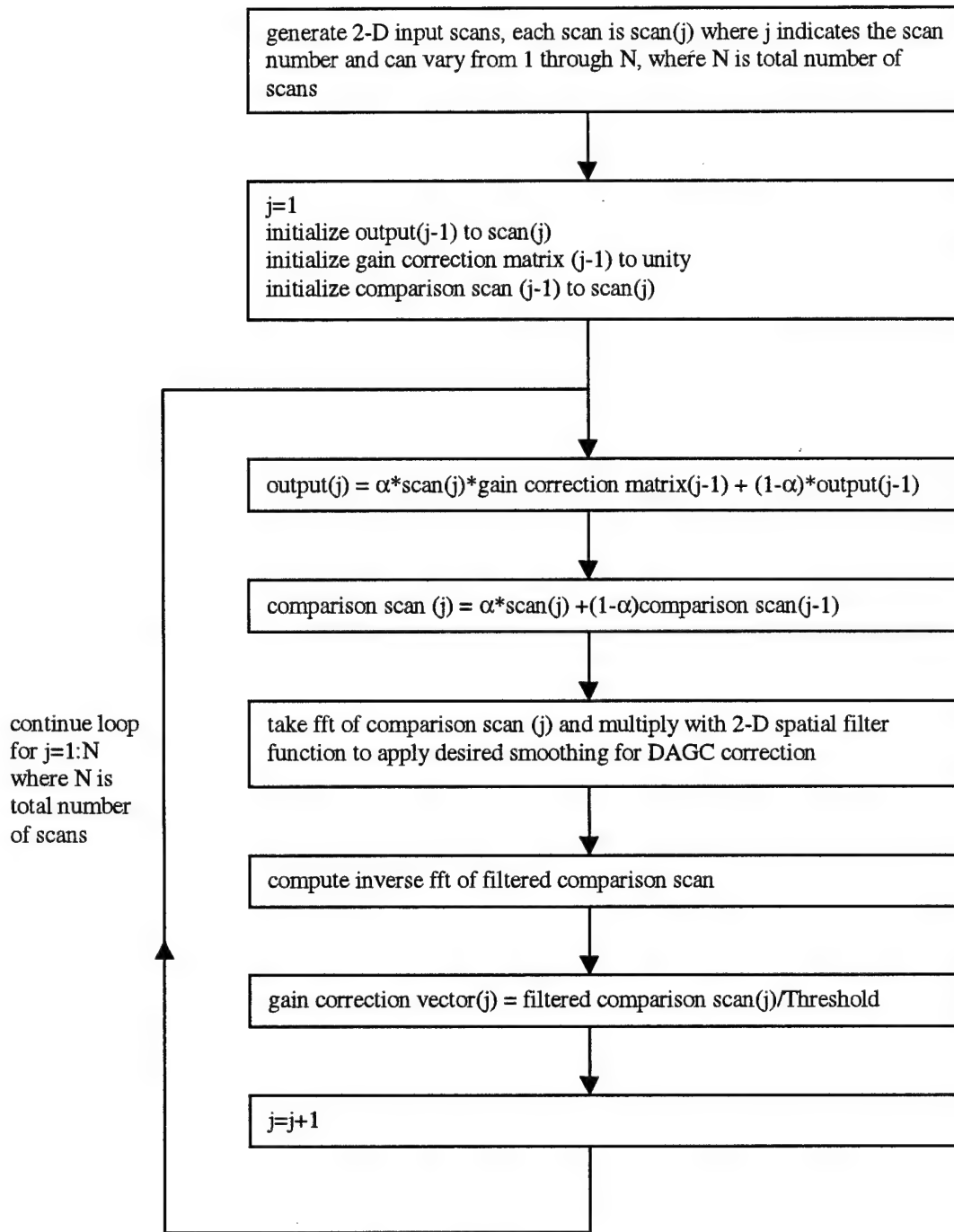


Figure 16: Flow chart for algorithm corresponding to DAGC processing module.

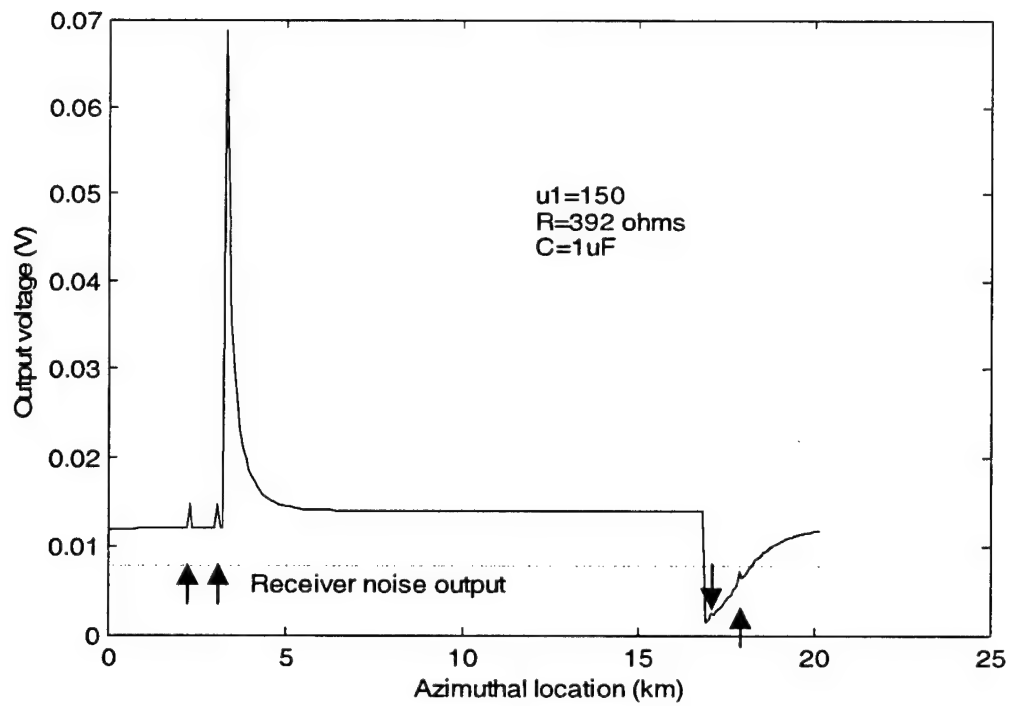


Figure 17: Output from AAGC for configuration 1 deterministic input signal. Arrows identify targets.

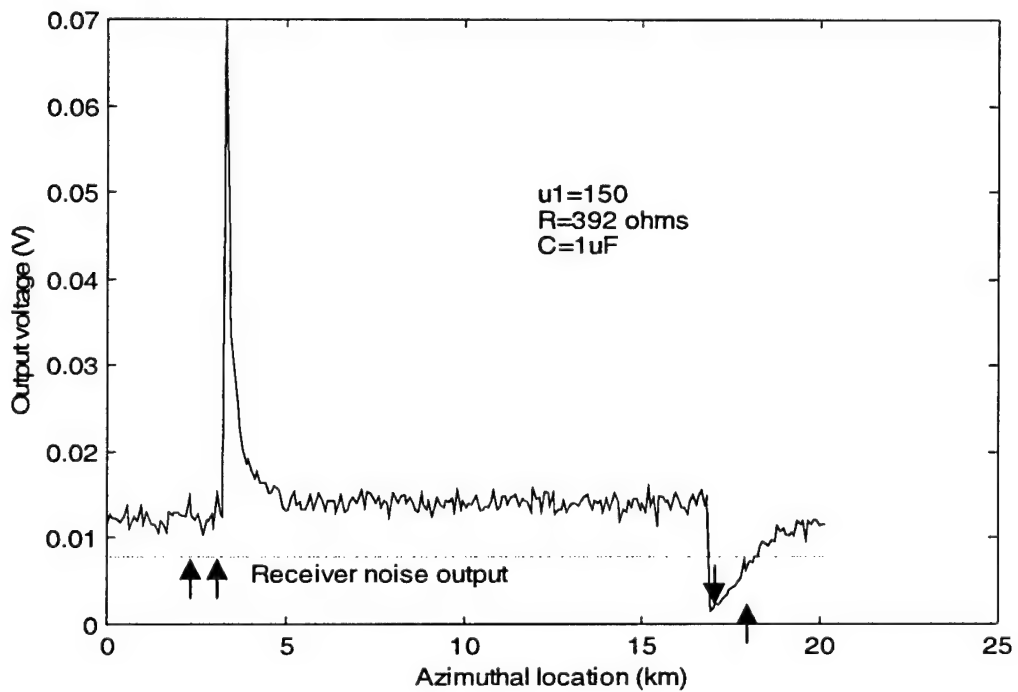


Figure 18: Output from AAGC for configuration 1 with non-deterministic input signal added. Arrows identify targets.

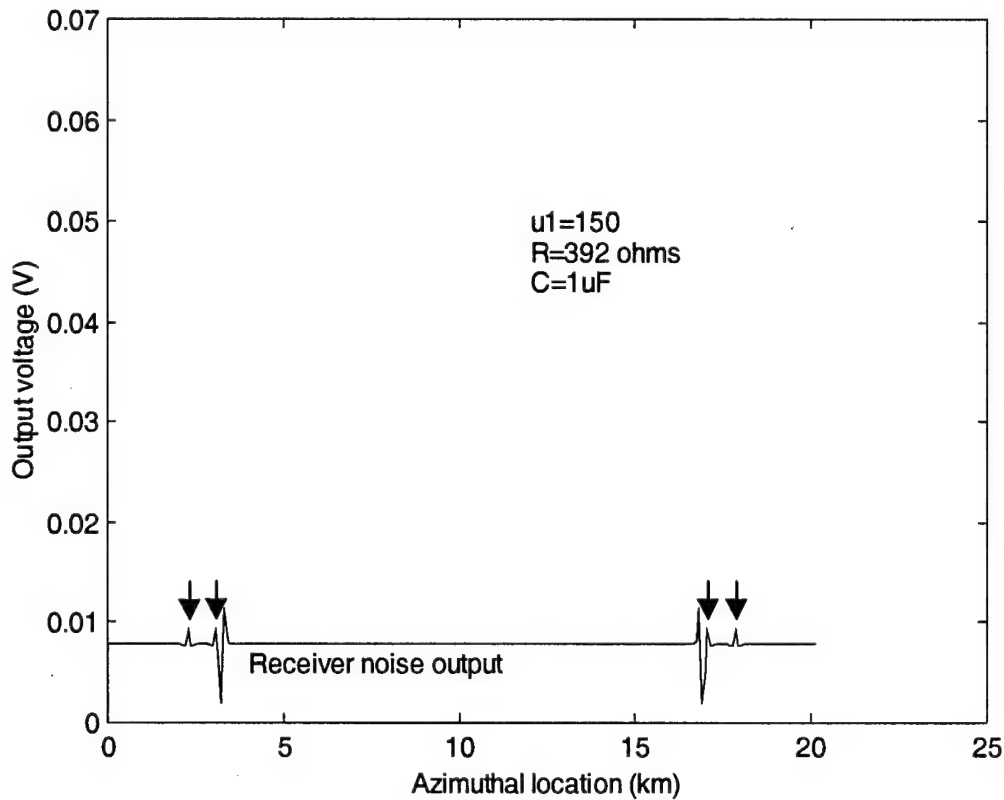


Figure 19: Plot along azimuthal vector containing targets of DAGC output for configuration 1 with deterministic input data. Arrows indicate targets.

contrast to the non-symmetric response of the AAGC where clear identification of the targets right up to the land-sea transition on the leading edge is achieved at the cost of significant masking on the trailing edge. It is also apparent that targets closer to the land-sea transitions, i.e. within the filter's 200 m radius, would suffer from masking under the DAGC systems. Roughly speaking, spatial filtering on the clutter map under the DAGC scheme rather than the real time approach of the AAGC allows the response lag to be symmetrically distributed across the land-sea boundary thereby cutting in half the extent of the shadow region on the trailing edge if an identical filter width is assumed in both approaches. Of course, as mentioned earlier, this comes at the expense of the addition of a shadow zone on the leading edge of the land-sea transition. In addition, it is unlikely that the DAGC and AAGC will have identical filter responses although due to the digital nature of the DAGC system it is possible to choose and implement any desired filter response.

The non-symmetrical AAGC and symmetrical DAGC behaviour was anticipated and was the primary motivation for investigating the use of the DAGC. The resolution of the AAGC system can be improved by decreasing the capacitance of the RC filter. Figure 20 illustrates the effect of reducing the capacitance by two orders of magnitude to $0.01 \mu\text{F}$. Practically, the manipulation of the capacitance of the range gated filter banks is very difficult under actual operation and it is not possible to adjust the capacitance to match the varying pulse repetition and scanning rates used in the different modes of operation. This typically results in the choice of a compromise value and the resulting non-optimal performance of all modes. In contrast, manipulation of the DAGC parameters is trivial as the filtering operation is performed digitally and operating parameters are easily adjusted within the software.

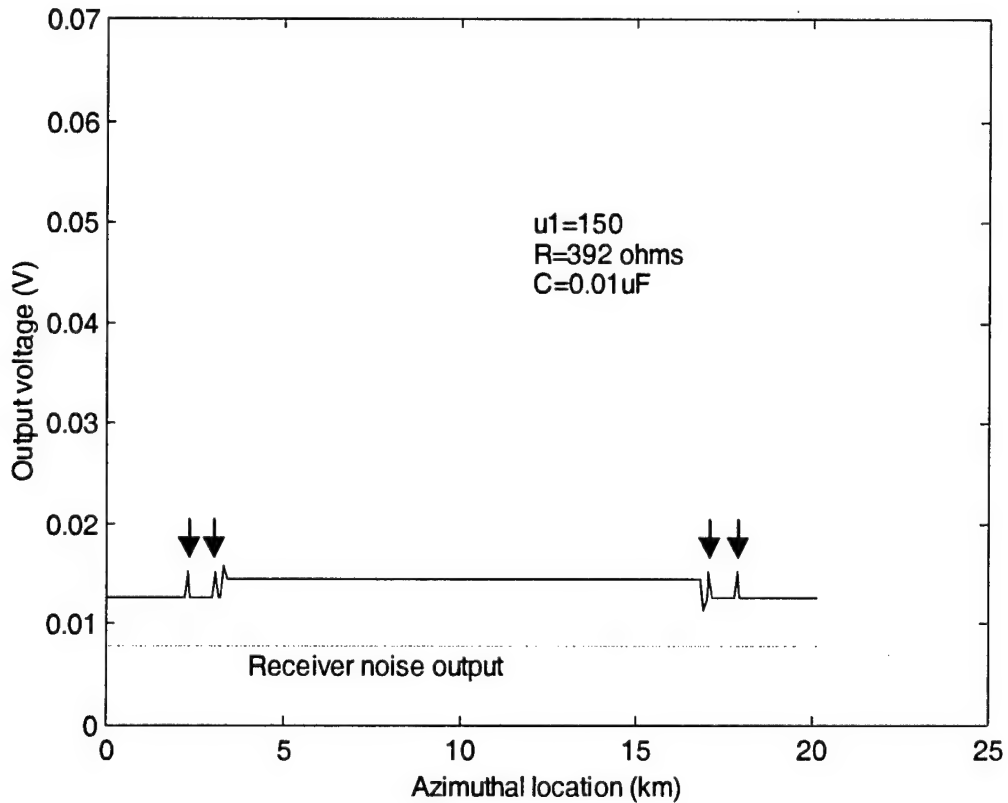


Figure 20: Output from AAGC for configuration 1 deterministic input signal with capacitance reduced by two orders of magnitude in RC filter. Arrows indicate targets.

Figure 21 shows the output with the non-deterministic portion of the clutter signal added using an alpha of 0.025 in equation 3.1 above. Comparing figures 18 and 21 the performance improvement on the trailing edge and small degradation on the leading edge under DAGC processing is readily apparent.

Another desirable feature of the DAGC approach is the excellent regulation of the return signal across the full field of view. Other than small transition regions where the box filter straddles the sea land interface, the output is perfectly flat (ignoring the non-deterministic portion of the clutter) and exactly equal to the

desired quantization level, which is that due to the intrinsic receiver noise temperature alone. By contrast the output from the AAGC loop is imperfectly regulated, and while the dynamic range between the sea clutter and land clutter is greatly reduced there is still a 1.2 db difference and in both cases the output is above that due to receiver noise alone. While the regulation response of the AAGC can be improved by increasing the gain in the feedback arm (or alternately by increasing the input signal strength into the loop see table 2.1), this requires the loop to be operated at a higher attenuation level. This may exceed the maximum dynamic range of the voltage controlled attenuators (or equivalently amplifiers) and also require adjustment to the other gains in the input chain. This type of adjustment proves difficult in actual systems and introduces the possibility of operator error.

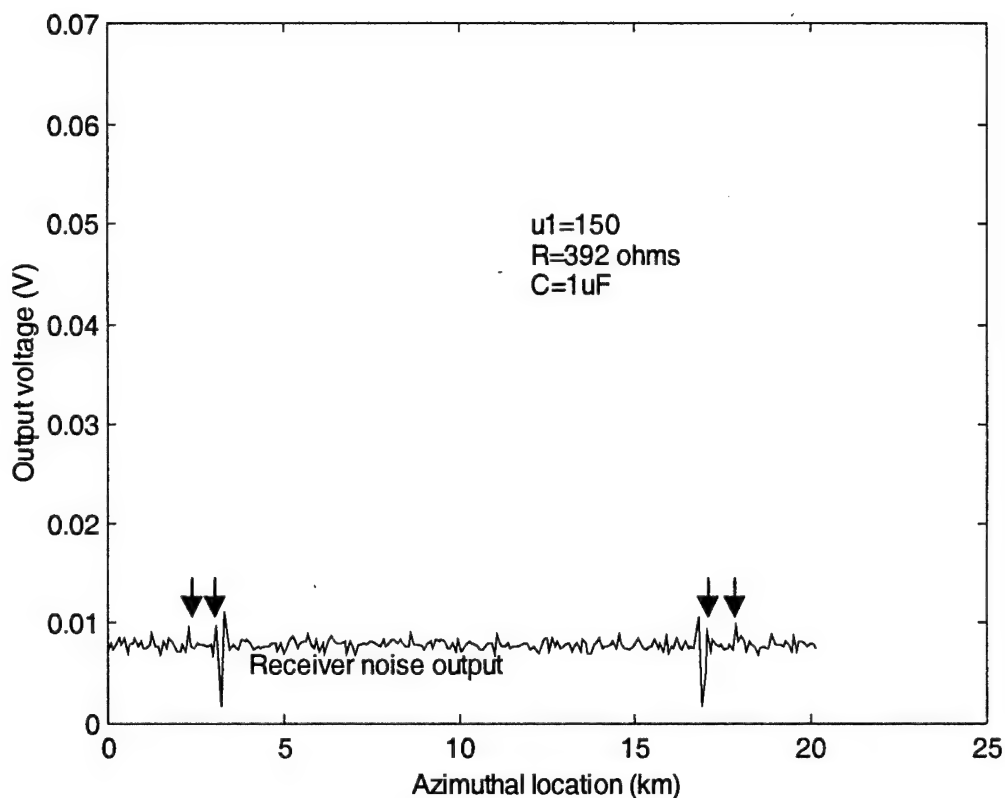


Figure 21: Plot along azimuthal vector containing targets of DAGC output for configuration 1 input data with non-deterministic portion of clutter signal added. Arrows indicate targets.

It should be noted that the improved resolution of the DAGC approach implemented in this report comes at the expense of reduced detection probability in regions where the fine resolution is not required. This occurs due to the small spatial extent of the 'box' filter used to extract the gain correction signal from the clutter map. The smaller the spatial dimensions of the filter used the more heavily the actual target will contribute to the gain correction matrix in the region around the target. Hence the gain in this region will

be pulled down by the presence of the target thereby reducing the final output signal strength of the target and its detection probability. This is also true for the AAGC system. If the time constant of the RC filter is decreased to allow the response to adjust more quickly to a land-sea transition then more of the high frequency components associated with the target signal will be suppressed by the AAGC resulting in similar reductions in the signal target strength.

3.2 Configuration 2 Simulations - RADAR Sweeping Parallel to Land

Configuration 2 investigates the effect of the finite sampling window of the range gated filtering employed by the AAGC system. Each range gate filter is assumed to sample the incoming signal for $3.8 \mu\text{s}$, corresponding to a range length of approximately 570 m. For the near target located 225 m from shore the worst case scenario will occur when the range sampling interval lies approximately half on land and half on sea surface thereby just containing the target within its limits. Under these conditions it is sufficiently accurate to assume that the feedback signal after the RGF will equal the DC average across the range sampling interval as the higher frequency components of the variation across this window are heavily filtered by the RGF.

Figure 22 displays the AAGC outputs along a range vector through targets located 225 and 975 m from the shoreline. The worst case scenario outlined above has been assumed. The transition between range sampling intervals lying entirely over the sea and the one straddling the land sea interface is clearly visible in the drop in signal levels between the two traces. This figure can be contrasted with figure 23 for the DAGC. Since the range and azimuth bin intervals of the digital data are similar in size, and the filtering operation is symmetrical in the range and azimuth directions, the DAGC output of figure 23 is essentially the same as that shown in figure 21. Theoretically, the azimuthal resolution of the AAGC method could be improved by decreasing the range sampling interval but practical considerations limit the total physical number of range sampling filters that can be implemented.

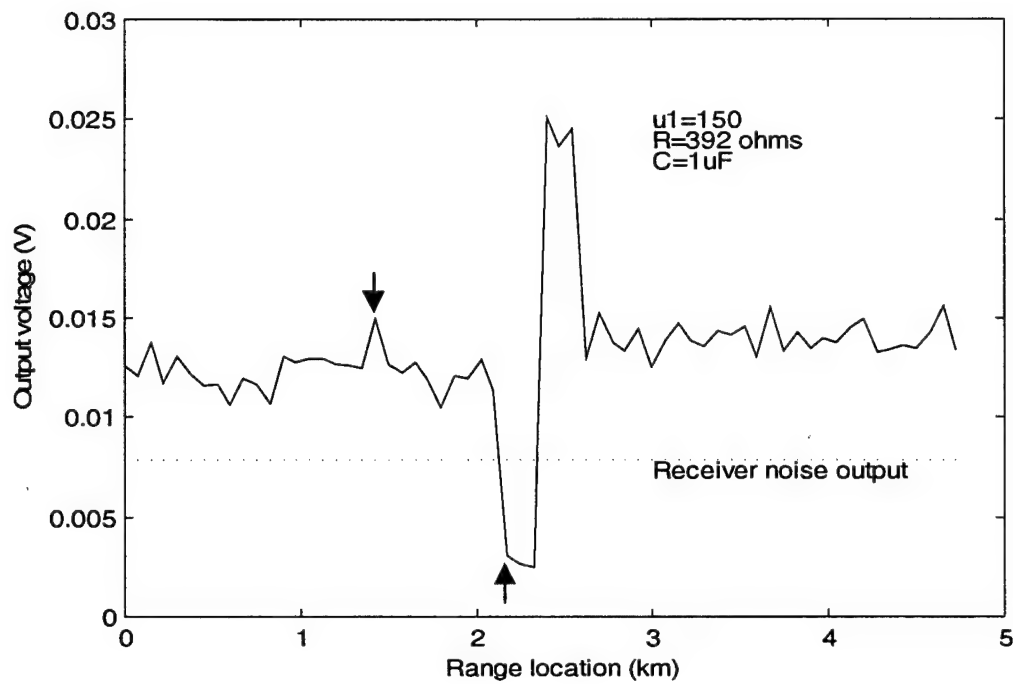


Figure 22: Plot along range vector containing targets of AAGC output for configuration 2 input data with non-deterministic portion of clutter signal added. Arrows indicate targets.

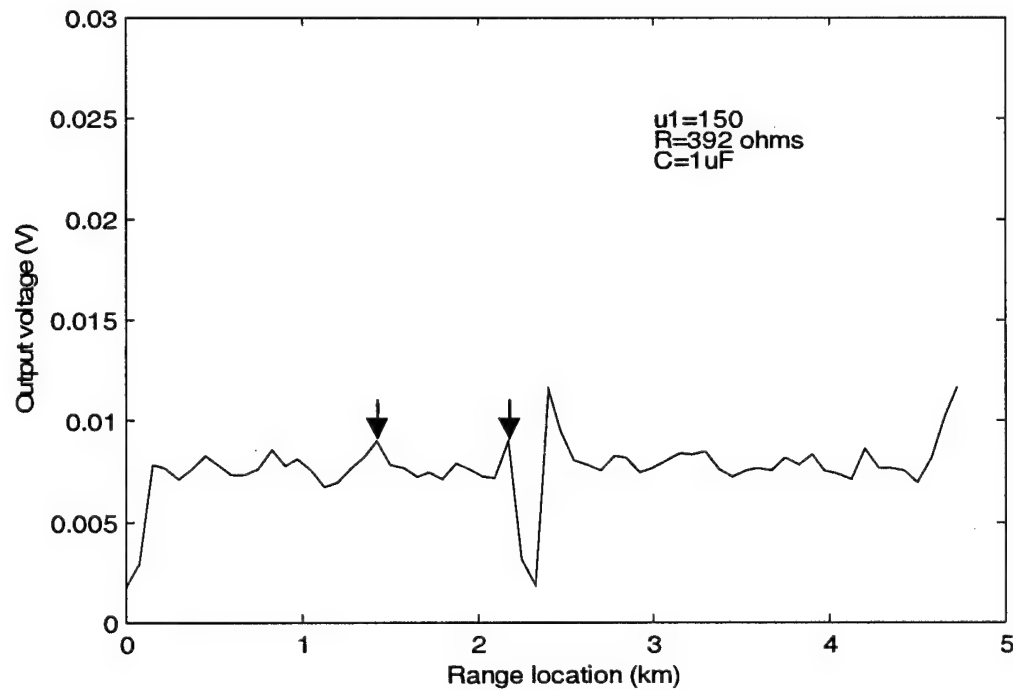


Figure 23: Plot along range vector containing targets of DAGC output for configuration 2 input data with non-deterministic portion of clutter signal added. Arrows indicate targets.

4.0 Summary and Future Work

In summary, the use of the DAGC system balances the output response across the leading and trailing edges of regions with large cross section variations, providing a symmetrical response. This is accomplished at the expense of an increased shadow zone on the leading edge of a sea to land transition over that of the AAGC response but with a significant improvement over the AAGC trailing edge response. In general, the dramatic improvement at the trailing edge justifies the small performance penalty at the leading edge. The uniform performance of the DAGC across the field of view also simplifies interpretation of the output.

One of the major advantages of a digital processing system over the hard wired AAGC approach is the ability of the DAGC system to be adjusted to optimize the output for any particular mode of RADAR surveillance. This ability alone is strong justification for considering the adoption of a DAGC system.

As discussed in the report, other considerations such as relative stability of the two systems and noise behaviour do not strongly recommend one method over the other. Both systems should remain stable over the range of conditions likely to be encountered during operation and the small decrease in signal to noise ratio at the output of the DAGC in comparison with the AAGC system is likely to be much less than 5% for any practical implementation utilizing temporal averaging and spatial filtering of the clutter map.

No attempt has been made in this report to quantify improvements or decreases in detection probability that would occur with the implementation of a DAGC scheme. In order to do this it is necessary to identify the detection scheme being used. One focus of future investigations should be to quantify the expected behaviour of the DAGC system using different CFAR and peak detection schemes. In addition, the use of more elaborate statistical noise models such as the K-distribution should provide a clearer picture of performance under more realistic conditions. Any such analysis would also benefit from the inclusion of other practical receiver dependent parameters such as bandwidth, pulse compression etc.

The flexibility of the digital processing scheme also opens the possibility for real time manipulation of the implemented filter function. It is envisioned that the potential exists to use edge finding techniques to modify the spatial shape of the filter interactively to prevent the filter from straddling the land-sea boundaries and thereby further reduce the shadow zone along the coast line.

Future work will focus on developing the basic AAGC and DAGC processing code into modules which can be used in conjunction with the DREO GMTI simulator to allow pre-development modeling of receiver designs and allow ongoing development and testing of detection schemes.

References

- [1] B.M. Oliver, "Automatic Volume Control as a Feedback Problem", Proc. IRE, vol. 36, pp. 466-473, 1948
- [2] A. Damini, "Digital Scan Conversion Algorithms for Ground based and Airborne RADARS (U), DREO Report No. 1113, December 1991.
- [3] B.C. Kuo, "Digital Control Systems", Holt, Rinehart and Winston Inc., Toronto, 1980.
- [4] R.C. Dorf, "Modern Control Systems", Addison-Wesley Publishing Company, Don Mills, 1992.

List of Acronyms

DND	Department of National Defence
AAGC	Analog Automatic Gain Control
AGC	Automatic Gain Control
DAGC	Digital Automatic Gain Control
DSC	Digital Scan Converter
PRF	Pulse Repetition Frequency
RC	Resistance*Capacitance
RGF	Range Gated Filter

DOCUMENT CONTROL DATA

(Security classification of title, body of abstract and indexing annotation must be entered when the overall document is classified)

1. ORIGINATOR (the name and address of the organization preparing the document. Organizations for whom the document was prepared, e.g. Establishment sponsoring a contractor's report, or tasking agency, are entered in section 8.)

DEFENCE RESEARCH ESTABLISHMENT
DEPARTMENT OF NATIONAL DEFENCE
OTTAWA ONTARIO CANADA K1A 0K2

2. SECURITY CLASSIFICATION
(overall security classification of the document, including special warning terms if applicable)

UNCLASSIFIED

3. TITLE (the complete document title as indicated on the title page. Its classification should be indicated by the appropriate abbreviation (S,C or U) in parentheses after the title.)

DIGITAL AUTOMATIC GAIN CONTROL (DAGC) FOR SURVEILLANCE RADAR APPLICATIONS: THEORY
AND SIMULATION (U)

4. AUTHORS (Last name, first name, middle initial)

MC DONALD, MICHAEL K.

5. DATE OF PUBLICATION (month and year of publication of document)

NOV 2000

6a. NO. OF PAGES (total containing information. Include Annexes, Appendices, etc.)

36

6b. NO. OF REFS (total cited in document)

3

7. DESCRIPTIVE NOTES (the category of the document, e.g. technical report, technical note or memorandum. If appropriate, enter the type of report, e.g. interim, progress, summary, annual or final. Give the inclusive dates when a specific reporting period is covered.)

DREO REPORT

8. SPONSORING ACTIVITY (the name of the department project office or laboratory sponsoring the research and development. Include the address.)

DEFENCE RESEARCH ESTABLISHMENT OTTAWA
DEPARTMENT OF NATIONAL DEFENCE
OTTAWA, ONTARIO, CANADA, K1A 0K2

9a. PROJECT OR GRANT NO. (if appropriate, the applicable research and development project or grant number under which the document was written. Please specify whether project or grant)

3DB29

9b. CONTRACT NO. (if appropriate, the applicable number under which the document was written)

10a. ORIGINATOR'S DOCUMENT NUMBER (the official document number by which the document is identified by the originating activity. This number must be unique to this document.)

DREO TECHNICAL REPORT 2000-115

10b. OTHER DOCUMENT NOS. (Any other numbers which may be assigned this document either by the originator or by the sponsor)

11. DOCUMENT AVAILABILITY (any limitations on further dissemination of the document, other than those imposed by security classification)

- (x) Unlimited distribution
() Distribution limited to defence departments and defence contractors; further distribution only as approved
() Distribution limited to defence departments and Canadian defence contractors; further distribution only as approved
() Distribution limited to government departments and agencies; further distribution only as approved
() Distribution limited to defence departments; further distribution only as approved
() Other (please specify):

12. DOCUMENT ANNOUNCEMENT (any limitation to the bibliographic announcement of this document. This will normally correspond to the Document Availability (11). However, where further distribution (beyond the audience specified in 11) is possible, a wider announcement audience may be selected.)

13. ABSTRACT (a brief and factual summary of the document. It may also appear elsewhere in the body of the document itself. It is highly desirable that the abstract of classified documents be unclassified. Each paragraph of the abstract shall begin with an indication of the security classification of the information in the paragraph (unless the document itself is unclassified) represented as (S), (C), or (U). It is not necessary to include here abstracts in both official languages unless the text is bilingual).

The potential for using a digital automatic gain control (DAGC) is examined. The DAGC operates by digitally storing a clutter map of the average of past returns. This average clutter map is digitally filtered to remove small spatial variations and the resulting values are used to adjust the front end receiver gain. In contrast, a traditional analog automatic gain control (AAGC) uses real time filtered feedback to control the adjustable front end gain. The physical realizability constraints of an AAGC typically result in a wider shadow zone for regions where the scan is moving from a land to sea clutter environment. It is shown that the DAGC filtering operation on the clutter map of past returns allows the spatial extent of the filter to be distributed evenly across the land-sea transition regions thereby reducing the shadow zone. The AAGC is shown to display slightly superior noise performance over the DAGC approach. Simulations of the behaviour of both systems under simplified configurations are also shown to qualitatively illustrate and clarify the tradeoffs associated with either approach.

14. KEYWORDS, DESCRIPTORS or IDENTIFIERS (technically meaningful terms or short phrases that characterize a document and could be helpful in cataloguing the document. They should be selected so that no security classification is required. Identifiers such as equipment model designation, trade name, military project code name, geographic location may also be included. If possible keywords should be selected from a published thesaurus. e.g. Thesaurus of Engineering and Scientific Terms (TEST) and that thesaurus-identified. If it is not possible to select indexing terms which are Unclassified, the classification of each should be indicated as with the title.)

CLUTTER MAP
AUTOMATIC GAIN CONTROL